Mineralogy and Petrology (2019) 113:533–553
https://doi.org/10.1007/s00710-019-00664-0

ORIGINAL PAPER

The new mineral fluorbarytolamprophyllite, $(Ba,Sr,K)_2[(Na,Fe^{2+})_3TiF_2][Ti_2(Si_2O_7)_2O_2]$ and chemical evolution of lamprophyllite-group minerals in agpaitic syenites of the Kola Peninsula

Maria I. Filina[1] · Sergey M. Aksenov[2,3] · Natalia V. Sorokhtina[1] · Nikita V. Chukanov[4] · Natalia N. Kononkova[1] · Dmitriy I. Belakovskiy[5] · Sergey N. Britvin[6] · Lia N. Kogarko[1] · Alexandr D. Chervonnyi[5] · Ramiza K. Rastsvetaeva[2]

Received: 11 October 2017 / Accepted: 20 March 2019 / Published online: 25 April 2019

Abstract

Unusual agpaitic syenites containing up to 25 vol.% lamprophyllite-group minerals (lamprophyllite, fluorlamprophyllite, barytolamprophyllite, and the new mineral species fluorbarytolamprophyllite, IMA 2016–089) have been discovered in the Niva intrusion and Mokhnatye Roga alkaline dyke belonging to the Kola Alkaline Province, northwestern Russia. The other main components of the rocks are potassium feldspar, Ti-rich aegirine-augite, aenigmatite, alkaline amphiboles, astrophyllite, natrolite, and ferripyrophyllite. Three generations of lamprophyllite-group minerals can be distinguished based on their morphological features. The new mineral fluorbarytolamprophyllite is the F-dominant analogue of barytolamprophyllite and the Ba-dominant analogue of fluorlamprophyllite. It represents the early generation of lamprophyllite-group minerals (LGM) and forms brown prismatic crystals, their radial aggregates and marginal zones of fluorlamprophyllite crystals. The lustre of the new mineral is vitreous to pearly. Mohs hardness is 2.5. D_{calc} is 3.662 g/cm^3. The mineral is optically biaxial (+), $\alpha = 1.738(3)$, $\beta = 1.745(4)$, $\gamma = 1.777(4)$ (589 nm), 2 V (meas.) = 55(5)°, 2 V (calc.) = 51°. The chemical composition (electron microprobe, water determined by TGA, wt.%) is: Na_2O 10.01, K_2O 2.65, MgO 0.43, CaO 0.64, SrO 5.59, BaO 16.23, MnO 0.50, FeO 4.44, Al_2O_3 0.08, TiO_2 27.31, ZrO_2 0.22, Nb_2O_5 0.91, Ta_2O_5 0.15, SiO_2 29.35, F 2.41, H_2O 0.26, total 101.18. The empirical formula based on 18 anions is $(Ba_{0.865}Sr_{0.44}K_{0.46}Na_{0.26})_{\Sigma 2.025}(Na_{2.38}Ca_{0.09}Fe_{0.47}Mn_{0.06})_{\Sigma 3.00}(Ti_{2.79}Mg_{0.09}Fe_{0.035}Nb_{0.06}Zr_{0.015}Ta_{0.01})_{\Sigma 3.00}(Si_{3.99}Al_{0.01})_{\Sigma 4.00}O_{16}[F_{1.04}O_{0.72}(OH)_{0.24}]_{\Sigma 2.00}$. The IR spectrum is given. The strongest lines of the powder X-ray diffraction pattern are [d, Å (I,%) (hkl)]: 9.692 (40) (200), 3.726 (59) (−311), 3.414 (67) (311), 3.230 (96) (300), 3.013 (53) (−5–11), 2.780 (100) (221), 2.662 (52) (002). The crystal structure has been solved and refined to $R_1 = 5.07$ based on 2897 independent reflections with $I > 2\sigma(I)$. Fluorbarytolamprophyllite is monoclinic, space group $C2/m$. The unit-cell parameters refined from the powder data are: $a = 19.520(5)$, $b = 7.0995(17)$, $c = 5.3896(20)$ Å, $\beta = 96.657(23)°$; $V = 741.86(24)$ Å^3, $Z = 2$. At Niva and Mokhnatye Roga, most of the LGM were formed during magmatic stage of syenite crystallization from alkaline melt enriched in Na, K, Ba, Fe, Ti and F. Compositional variation of the examined LGM and their textural

Editorial handling: L. Danyushevsky

Electronic supplementary material The online version of this article (https://doi.org/10.1007/s00710-019-00664-0) contains supplementary material, which is available to authorized users.

✉ Sergey M. Aksenov
aks.crys@gmail.com

[1] Vernadsky Institute, Russian Academy of Sciences, Kosygin Street 19, Moscow 119991, Russia

[2] FSRC "Crystallography and Photonics", Russian Academy of Sciences, Leninsky Prospekt 59, Moscow 119333, Russia

[3] Present address: Department of Civil & Environmental Engineering & Earth Sciences, University of Notre Dame, Notre Dame, IN 46556, USA

[4] Institute of Problems of Chemical Physics, Russian Academy of Sciences, Chernogolovka, Moscow region 142432, Russia

[5] Fersman Mineralogical Museum, Russian Academy of Sciences, Leninsky Prospekt 18/2, Moscow 119071, Russia

[6] Department of Crystallography, Institute of Earth Sciences, St. Petersburg State University, University Emb. 7/9, St. Petersburg 199034, Russia

relations show changes in the Sr/Ba ratio in the parental melt and increasing activity of F and Ba in derivatives fluids as the main factors driving this variation.

Keywords Fluorbarytolamprophyllite · New mineral · Heterophyllosilicate · Lamprophyllite group · Agpaitic syenite · Kola alkaline province

Introduction

Titanium-rich members of the lamprophyllite-group minerals (LGM) (Rastsvetaeva et al. 2016) are common in a wide spectrum of igneous rocks, including intrusive and effusive alkaline rocks; related pegmatites; pneumatolytic and other rocks formed during late crystallization stages of alkaline and alkaline–ultrabasic-carbonatite complexes; and lamproites. These minerals are often found in nepheline syenites and related pegmatites, e.g. at Inagli and Botogol in Russia (Labeznik et al. 1998; Chukanov et al. 2004; Kapustin 1973), Pilanesberg in South Africa (Zaitsev and Kogarko 2002), Mont Saint-Hilaire in Canada (Wight and Chao 1995), Bearpaw Mountains and Gordon Butte in the United States (Chakhmouradian and Mitchell 1999, 2002), and Poços de Caldas in Brazil (Ulbrich 1993). They were also discovered in other alkaline rock types: ijolite pegmatites of the Gardiner complex, Greenland (Johnsen et al. 1994), peralkaline nephelinite lava of the Oldoinyo Lengai volcano, Tanzania (Dawson 1998), alkaline basalts of the Eifel paleovolcanic region, Germany (Chukanov et al. 2011, 2012, 2014), fenites of the Sarambi carbonatite complex, Paraguay (Haggerty and Mariano 1983), phlogopite-rich pegmatites of a lamproite-like intrusion in the Wajrakarur kimberlite field, India (Kaur and Mitchell 2013).

The Kola alkaline province (Fig. 1) includes more than 20 alkaline and alkaline-ultramafic-carbonatite intrusive complexes (Kukharenko et al. 1965; Gerasimovskii et al. 1966; Zhirov 2015). LGM from nepheline syenites, lujavrites, malignites, peralkaline pegmatites and hydrothermalites were described in Lovozero, Khibiny, Niva alkaline massifs and Kovdor alkaline-ultramafic-carbonatite complex (Arzamastsev et al. 1999, 2000; Azarova 2004; Zaitsev and Kogarko 2002; Ivanyuk et al. 2002; Chukanov et al. 2004; Moiseev and Chukanov 2006; Akimenko et al. 2014, 2015). LGM occur as minor or accessory minerals in igneous rocks and can be major or minor components of hydrothermal and pegmatite associations.

The first petrological and mineralogical descriptions of agpaitic rocks and LGM from the Niva intrusion and the Mokhnatye Roga dyke situated in the Kola Peninsula were given by Arzamastsev et al. (1999, 2000) and Akimenko et al. (2014, 2015). This paper describes unusual agpaitic syenites containing up to 25 vol.% LGM including lamprophyllite, fluorlamprophyllite, barytolamprophyllite, and the new mineral species fluorbarytolamprophyllite. We also discuss the main trends of compositional evolution of LGM from these two localities, and provides comparisons with other alkaline rocks enriched in Na, K or Ca.

The new mineral fluorbarytolamprophyllite $(Ba,Sr,K)_2[(Na,Fe^{2+})_3TiF_2][Ti_2(Si_2O_7)_2O_2]$, is a high-fluorine analogue of barytolamprophyllite-2 *M* $(Ba,Sr,K)_2[Na(Na,Mn)_2Ti(OH)_2][Ti_2(Si_2O_7)_2O_2]$, which can also be considered as a Ba-dominant analogue of fluorlamprophyllite $(Sr,Na)_2[(Na,Mn)_3(Ti,Fe)F_2][Ti_2(Si_2O_7)_2O_2]$. The name of the new mineral is given on the basis of compositional similarities with barytolamprophyllite. The mineral and its name have been approved by the IMA Commission on New Minerals, Nomenclature and Classification (IMA no. 2016–089). The type specimens are deposited in the collection of the Fersman Mineralogical Museum of the Russian Academy of Sciences, Moscow, Russia, with the registration numbers 4916/1 and 4916/2.

Occurrence and geological features

The Kola-Karelian alkaline province (KKAP) situated in the Kola Peninsula, northern parts of the Republic of Karelia, and adjacent parts of Finland, is one of the largest alkaline provinces in the world (Fig. 1). KKAP is situated within three Archean to Proterozoic (2.9–1.7 Ga) terranes (Daly et al. 2012). Alkaline magmatic activity reached its peak in the Devonian. The largest alkaline complexes Lovozero and Khibiny, and many alkaline-ultrabasic massifs with carbonatites were formed during this time over an area of more than 100,000 km^2, and their formation was connected to plume magmatism and related mantle-lithospheric geodynamic processes, as evidenced by numerous geological and isotopic data (Ernst and Bell 2010; Kogarko et al. 2009). According to the modern geological, morphometric and tectonophysical studies of the Kola-Karelian region, the Paleozoic carbonatite and alkaline massifs are located in areas with similar tectono-structural controls such as linear zones of deep faults and the main lineament of the Kandalaksha Graben (Fig. 1) (Kukharenko et al. 1965; Zhirov 2015). It is known, that activation of the upper mantle on Kola Peninsula at the Paleozoic time was the result of Plume-lithosphere interaction (Arzamastsev et al. 2001). More than 20 alkaline-ultrabasic and alkaline massifs were formed at

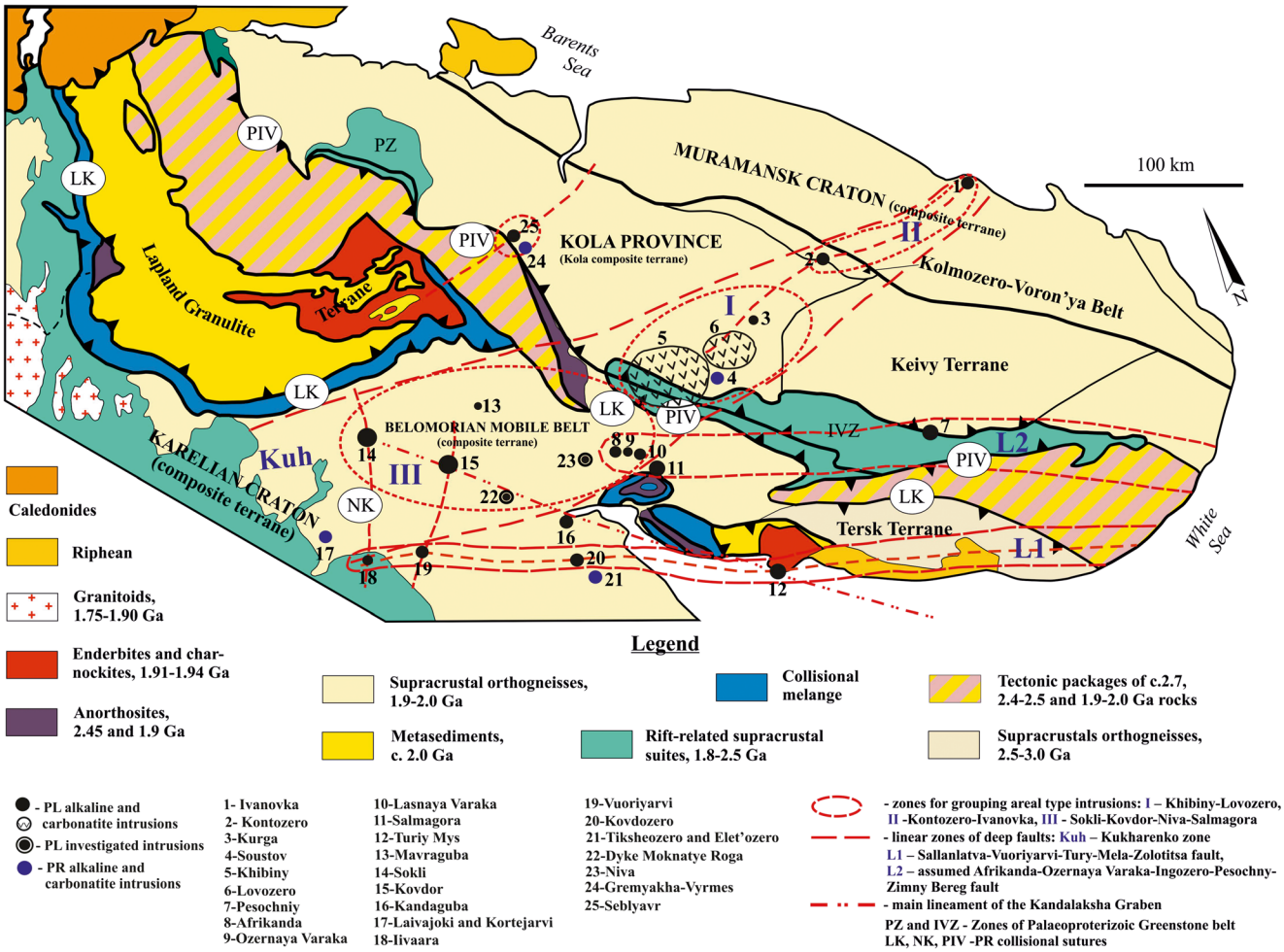

Fig. 1 Schematic geological map of Kola Peninsula and adjacent regions of northern Fennoscandia showing of alkaline, alkali-ultrabasic with carbonatites massifs with respect to the main tectonic structures (Daly et al. 2012, Zhirov 2015)

this time. The central part of this plume is located in Zone I on the map (Fig. 1) and includes Lovozero and Khibiny super large alkaline intrusions while Zones II and III are structural units of the next level correspond to the flows of thermal mass transfer and tectonic zones of localization of another and smaller alkaline and carbonatite massifs.

The Niva intrusion and the Mokhnatye Roga dyke are located in a zone controlled by a system of deep-seated faults (Fig. 1). Large carbonatite intrusions (Sokli, Kovdor, Afrikanda, Ozernaya Varaka, Lesnaya Varaka, Niva, Salmagora) and numerous associated dykes of different composition (lamprophyres, nephelinites, phonolites *etc.*) are also located in this zone (Arzamastsev et al. 2009).

The holotype sample of fluorbarytolamprophyllite was collected from the Niva agpaitic syenite intrusion discovered by Arzamastsev et al. (2000). This intrusion is situated ~50 km southwest of the Khibina intrusion (67°15′ N; 32°17′ E). It forms a lense-like body 1.5–2 km in diameter, which outcrops over an area of 600 m^2 on the southern shore of the Imandra Lake. The age of the massif is 383 ± 58 Ma as determined by the Sm-Nd method. The host rock of the Niva intrusion is Precambrian amphibole-biotite gneiss.

The co-type material with fluorbarytolamprophyllite was collected from agpaitic syenite of the Mokhnatye Roga dyke discovered in 2010 during mapping in the Kovdor area (Akimenko et al. 2014). The dyke is located about 35 km southwest of the Niva intrusion (67°15′ N, 31°30′ E), it is 4 km long and 160 m thick, striking east and dipping steeply (60°–90°) to the north. The host rocks of the dyke are Archean amphibole-biotite gneisses with interlayers of amphibolites.

Petrography of the rock-forming minerals

Agpaitic syenites from both occurrences are fine- to medium-grained green-colored rocks. The rock-forming minerals are potassium feldspar (25–30 vol.%), Ti-rich aegirine-augite (10–15 vol.%), aenigmatite (10–15 vol.%), amphiboles (5–10 vol.%), natrolite (10–15 vol.%) and LGM, including lamprophyllite, fluorlamprophyllite, barytolamprophyllite, and

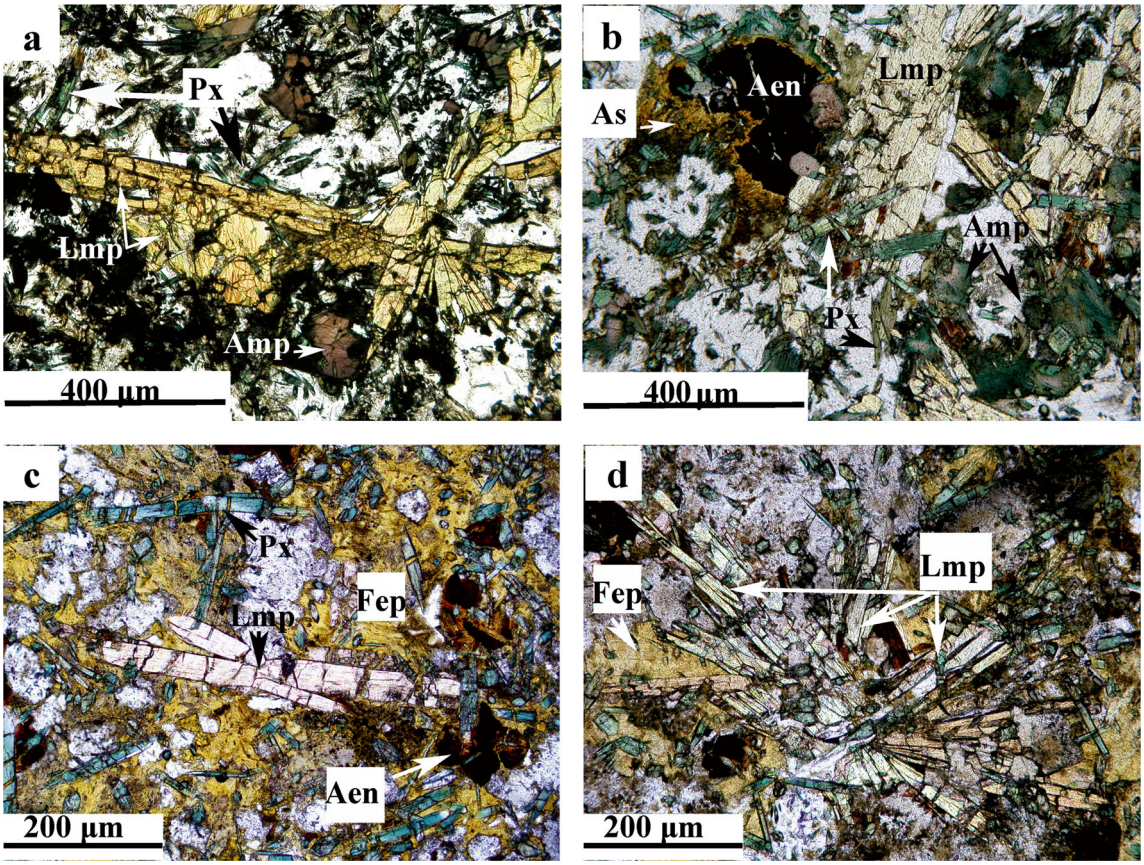

Fig. 2 Microphotographs (plane polarized light) showing structural characteristics of agpaitic syenites. Intergrowth of prismatic crystals of LGM (Lmp) from agpaitic syenites of the Niva intrusion (**a**, **b**) and Mokhnatye Roga dyke (**c**, **d**) surrounded by acicular green crystals of Ti-rich aegirine-augite (Px) and subhedral zoned pinkish-brown crystals of arfvedsonite (Amp). The matrix is presented by white aggregates of feldspar and natrolite (Fep), yellow aggregates of ferripyrophyllite replace brown euhedral crystals of aenigmatite (Aen)

Table 1 Representative compositions (wt.%) of major minerals of the agpaitic syenites

	1	2*	3	4	5	6	7	8	9	10	11	12	13	14	15
	K-Feldspar		Pyroxenes				Amphiboles				Aenigmatite		Astrophyllite		Natrolite
Zone			C	R	C	R	C	R	C	R					
SiO_2	64.87	65.06	50.63	50.99	51.05	51.31	51.71	52.34	50.92	49.27	41.63	41.43	37.19	38.92	46.9
TiO_2	0.03		1.83	2.22	1.96	4.67	4.14	3.29	4.3	2.48	10.11	9.99	9.62	10.43	n.d.
Al_2O_3	18.95	17.96	0.9	0.81	0.65	0.59	1.43	0.63	1.43	0.19	0.27	0.45	0.60	0.43	25.02
FeO	0.06	0.17	14.14	17.13	15.06	20.32	16.39	20.65	16.48	29.41	37.70	38.84	32.53	31.82	0.15
MnO	0.03	n.d.	0.41	0.53	0.54	0.36	0.51	0.41	0.55	1.01	1.72	1.44	1.40	1.5	n.d.
MgO	0.05	n.d.	8.91	6.85	8.11	3.29	11.59	4.46	9.93	1.14	1.99	1.86	1.82	1.86	n.a.
CaO	0.02	0.05	17.66	13.96	16.18	6.36	2.43	9.28	2.47	0.11	0.04	0.09	0.17	0.48	n.d.
Na_2O	0.09	0.14	3.7	5.68	4.31	10.1	6.74	8.17	6.87	6.92	7.77	7.63	3.30	3.66	16.33
K_2O	16.58	16.99	0.06	0.07	n.d.	0.02	3.34	0.02	3.27	4.69	n.d.	0.01	7.00	6.84	n.d.
ZrO_2	n.a.	n.a.	0.27	0.93	0.34	0.40	0.14	1.02	0.00	0.05	0.04	n.d.	0.07	n.d.	n.d.
V_2O_3	n.a.	n.a.	0.13	0.33	0.19	0.31	n.a.	n.a.	n.a.	n.a.	0.15	n.d.	n.d.	n.d.	n.d.
Nb_2O_5	n.a.	n.a.	n.a.	n.a.	n.a.	n.a.	n.a.	n.a.	n.a.	n.a.	0.09	0.12	0.12	0.08	n.d.
SrO	n.d.	0.09	n.a.	n.a.	n.a.	n.a.	n.a.	n.a.	0.40	0.04	n.a.	n.a.	n.a.	n.a.	n.a.
BaO	0.03	n.a.	n.a.	n.a.	n.a.	n.a.	n.a.	n.a.	0.06	0.14	n.a.	n.a.	0.06	n.d.	n.a.
F	n.a.	n.a.	n.a.	n.a.	n.a.	n.a.	3.40	n.d.	2.55	0.01	0.15	0.11	0.44	0.25	n.a.
Total	100.71	100.46	98.64	99.50	98.39	97.73	101.82	100.27	99.23	95.46	101.66	101.97	94.38	96.27	88.40
–O=F	–	–	–	–	–	–	1.43	0.00	1.07	0.00	0.06	0.05	0.19	0.11	–
Total	–	–	–	–	–	–	100.39	100.27	98.16	95.46	101.60	101.92	94.19	96.16	–

1,3,4,7,8,11,13 – agpaitic dyke, 2,5,6,9,10,12,14,15- Niva intrusions. *- (Arzamastsev et al. 2000), C - central and R – rim of zoned grains; n.a. — not analyzed, n.d. — not detected

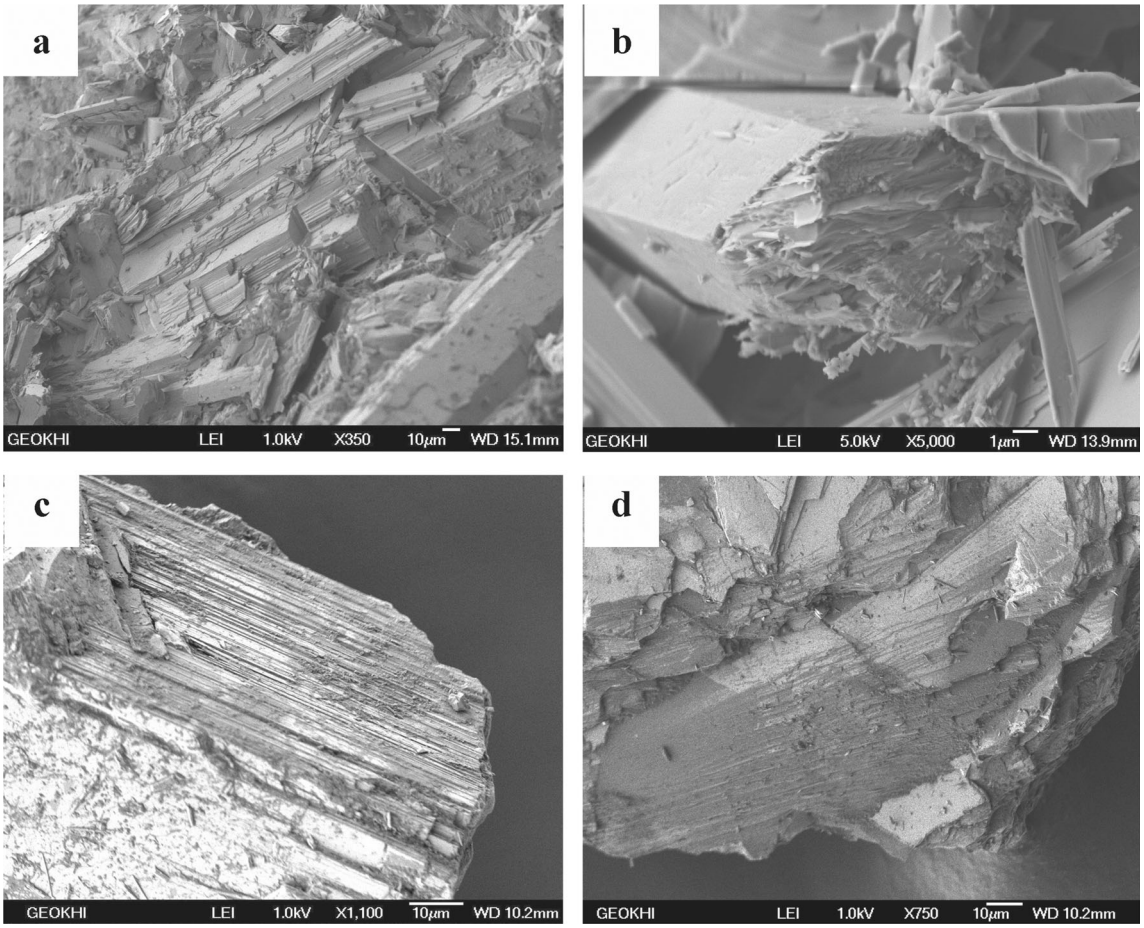

Fig. 3 Secondary electron images of representative morphology of LGM crystals from agpaitic syenites of the Niva intrusion (**a**, **b**) and Mokhnatye Roga dyke (**c**, **d**). (**a**) Intergrowth of prismatic crystals; (**b**) the internal structure of individual crystals; (**c**) polysynthetic twinning and (**d**) radiating aggregates of flattened prismatic crystals

fluorbarytolamprophyllite (up to 25 vol.% in total). Locally, the syenites contain hydrothermally altered sections, which contain up to 10 vol.% natrolite and ferripyrophyllite (Fig. 2 c,d). Astrophyllite, shcherbakovite, barite, an unidentified Mn carbonate, ilmenite, rutile and sulfides are the minor or accessory minerals. Syenite from the Niva intrusion contains more natrolite than that from the dyke. The following sequence of crystallization of the main minerals is observed in thin sections: potassium feldspar, Ti-rich aegirine-augite, aenigmatite, first generation of LGM, arfvedsonite, second and third generations of LGM, natrolite and ferripyrophyllite (the latter two minerals formed at postmagmatic, hydrothermal stage).

The results of electron microprobe analyses of the main rock-forming minerals are summarized in Table 1. According to the chemical composition and optical properties, potassium feldspar corresponds to orthoclase. Pyroxenes of the agpaitic syenites from both occurrences correspond to the diopside-hedenbergite-aegirine solid-solution system, typical for peralkaline rocks. Most pyroxene grains are normally zoned with contents of Na, Fe, and Ti increasing from core to rim, and Mg and Ca decreasing. Core compositions correspond to augite whereas rim compositions are Ti-rich aegirine-augite (Table 1). Some rims are close in composition to the aegirine end-member.

The amphiboles belong to the sodium-calcium and sodium groups. These minerals are zoned in composition: their cores are a pargasite-hastingsite solid-solution enriched in Ti, whereas the rims are arfvedsonite or potassic-arfvedsonite. Amphiboles have high F contents up to 3.4 wt.%. The amphiboles follow the same normal zoning trend as the pyroxenes.

Aenigmatite is a typical mineral of the examined rocks. It forms brownish red prismatic crystals up to 1 mm long. The mineral contains numerous inclusions of Ti-rich aegirine-augite and is often partly or completely replaced by yellowish orange astrophyllite or, rarely, by shcherbakovite. The composition of the rock-forming aenigmatite from the Niva syenite is similar to that in the dyke (Table 1).

Natrolite was identified on the basis of its chemical composition and infrared spectrum. Ferripyrophyllite forms radiating and scaly aggregates and was identified by optical properties in thin

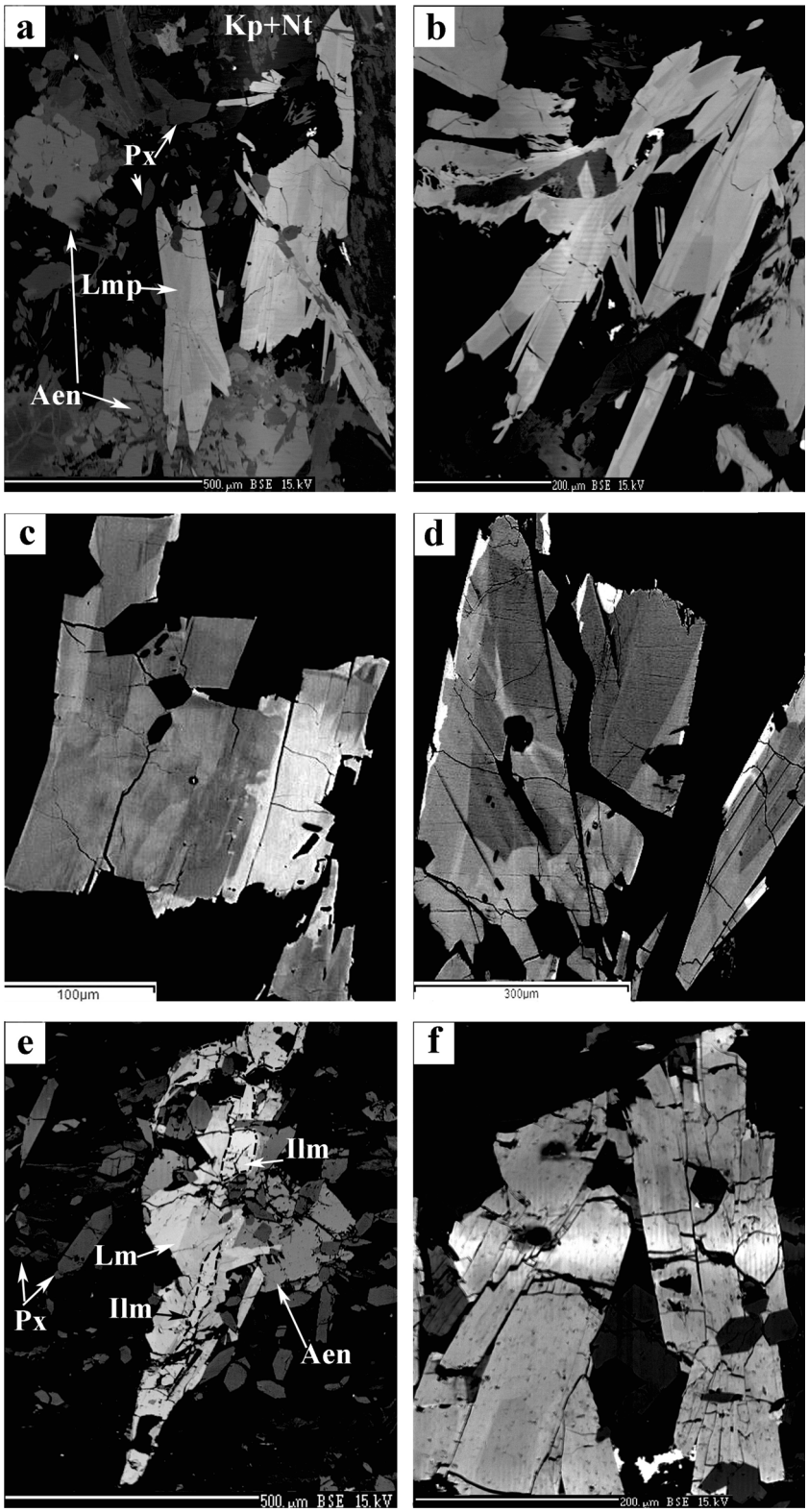

Fig. 4 BSE images of representative LGM (Lm) morphology and zoning from Niva intrusion (**a**-**d**) and Mokhnatye Roga dyke (**e**, **f**). (**a**-**e**) strongly zoned crystals with Ba-F-rich rim (light areas). (**e**) fractured LGM crystals with irregularly shaped grains of ilmenite (Ilm) in central zone. (**f**) slightly zoned LGM crystals of early generations

section and semi-quantitative microprobe analysis (SiO_2–48.89 wt.%; Fe_2O_3–31.35 wt.%, Al_2O_3–3.16 wt.%; MgO – 1.67 wt.%). The mineral have brownish yellow color, greenish-bright yellow pleochroism, the dispersion is weak: $r < v$.

Analytical methods

Information about the analytical methods is provided in Supplementary Information.

Table 2 Representative compositions of LGM from the Mokhnatye Roga dyke (wt.%)

	1	2	3	4	5	6	7	8	9	10	11	12	13	14
	crystal 1			crystal 2		crystal 3		crystal 4			crystal 5		crystal 6	crystal 7
	C	I	R	I	R	C	I	C	I	R	C	R	C	C
SiO_2	29.86	30.50	29.51	29.84	29.46	30.12	28.95	29.50	29.91	28.99	29.78	29.09	27.79	27.46
TiO_2	28.62	29.14	27.71	27.63	27.99	29.23	27.37	28.93	28.42	27.42	27.35	27.29	25.36	25.59
Al_2O_3	0.13	0.18	0.19	0.18	0.18	0.16	0.21	0.17	0.25	0.20	0.19	0.24	0.36	0.42
FeO	4.23	4.67	4.94	5.05	4.37	4.45	3.81	5.33	4.58	3.46	4.63	4.26	7.01	5.45
MnO	0.76	0.74	0.89	0.79	0.71	0.61	0.8	0.84	0.7	0.88	0.79	0.51	0.44	0.35
MgO	1.23	1.17	1.24	1.36	0.96	1.36	0.79	0.55	0.8	0.76	0.92	0.58	0.34	0.35
CaO	1.06	1.02	1.02	1.02	0.82	1.05	0.74	0.93	0.87	0.91	0.89	0.73	0.49	0.59
Na_2O	10.31	10.36	9.53	10.08	9.83	10.29	9.57	9.25	10.05	9.48	9.68	9.24	8.47	8.74
K_2O	1.40	1.68	1.72	1.76	2.12	1.40	2.1	2.76	2.24	2.11	1.96	3.07	3.11	2.93
BaO	6.83	8.64	9.95	9.63	11.42	6.71	13.23	12.30	12.82	14.65	12.97	16.03	13.92	16.39
SrO	11.72	10.88	9.83	9.32	8.71	12.57	8.3	6.64	8.12	7.71	8.49	4.21	5.54	5.17
ZrO_2	0.05	0.06	0.05	0.18	0.41	0.19	0.42	1.97	2.52	0.10	0.02	0.09	–	0.04
Nb_2O_5	0.13	0.12	0.24	0.06	0.78	0.14	0.79	0.28	0.29	0.23	0.41	1.05	1.63	1.59
Ta_2O_5	0.16	0.21	0.02	0.16	0.03	0.03	(0.01)	–	–	0.17	–	–	0.09	–
ThO_2	–	–	–	–	–	0.24	–	–	–	–	–	–	0.07	–
UO_2	–	–	–	–	–	0.17	–	–	–	–	–	0.59	–	–
F	2.11	2.41	2.66	3.22	2.91	2.31	2.43	1.97	2.52	2.21	2.28	2.03	1.2	2.16
Total	98.60	101.78	99.50	100.28	100.70	101.03	99.51	99.45	101.87	99.28	100.34	98.93	95.83	97.23
O = F	0.89	1.01	1.12	1.36	1.23	0.97	1.02	0.83	1.06	0.93	0.96	0.85	0.51	0.91
Total*	97.71	100.77	98.38	98.92	99.47	100.06	98.49	98.62	100.81	98.35	99.38	98.08	95.32	96.32

*recalculated for the concentration of fluorine. Analysis 1–7 is LGM generation I; 8–12 - generation II; 13–14 - generation III. Zones of crystals: C – core, R – rim, I –intermediate. — below detection limit. The contents for Ta_2O_5 of 0.01% by weight are given in brackets because they are close to the detection limit

Mineralogy and chemical composition of lamprophyllite-group minerals

LGM are the major components of the agpaitic syenites of the Niva intrusion and the Mokhnatye Roga dyke. Morphological and compositional data indicate the presence of three generations of these minerals in both occurrences (LGM-I, -II, and -III). The morphology and internal constitution of individual crystals and aggregates of the studied LGM are illustrated in Figs. 3 and 4. The earlier generations of LGM (LGM-I and -II) form large (2 to 5 mm long in the Niva intrusion and 1 to 3 mm long in the dyke) prismatic crystals showing distinct growth zoning in backscattered electron images (Fig. 4). The zones are characterized by different compositions, and may represent syntaxial intergrowths that are common for LGM (Rastsvetaeva et al. 2014). Some LGM crystals from the dyke contain relict inclusions of ilmenite in their central part (Fig. 4 e). In some cases, LGM-II form irregular grains associated with astrophyllite or shcherbakovite in the interstitial matrix. LGM-III occurs as smaller acicular crystals or their intergrowths with minerals of the late association: Nb-rich rutile, astrophyllite, shcherbakovite, Ca-Mn carbonates, sulfides, and barite. In addition, LGM-III forms the outer part of the early-generation LGM crystals. The color of all three generations varies from light to dark brown.

The chemical composition of the LGM from both occurrences changes during the successive crystallization of the three generations (Tables 2 and 3).

In the LGM-I crystals from the dyke and Niva intrusion, SrO concentrations increase from core to rim from 8.3 to 12.57 wt.% and 7.00 to 10.29 wt.%, respectively. BaO concentrations change in a similar manner, increasing from 6.83 to 13.23 wt.% and from 7.72 to 12.85 wt.%, respectively. LGM-I crystals are characterized by a maximum F concentration of 3.22 and 3.09 wt.%, respectively (Table 2 and 3).

In the LGM–II crystals, SrO concentrations decrease from 8.49 to 4.21 wt.% and from 8.08 to 3.34 wt.%, for dyke and Niva intrusion, respectively; the BaO content increases from 12.30 to 16.03 wt.% and from 13.32 to 19.99 wt.% (the rim of the crystals are characterized by the maximum Ba contents) (Tables 2 and 3). The F content also decreases in comparison with the LGM–I and maximal values are 2.43 and 2.74 wt.%.

The LGM–III crystals contain the largest BaO contents of 16.39 and 18.70 wt.%, for dyke and Niva intrusion, respectively, whereas SrO contents increase from 5.17 to 5.54 wt.% and from 5.17 to 6.51 wt.%. The F content varies from 2.16 to

Table 3 Formula coefficients of LGM from the Mokhnatye Roga dyke (*apfu*)

	1	2	3	4	5	6	7	8	9	10	11	12	13	14
$AO_{10–11}$ polyhedron														
Sr	0.91	0.82	0.77	0.72	0.68	0.96	0.66	0.52	0.62	0.62	0.66	0.34	0.46	0.43
Ba	0.36	0.44	0.53	0.50	0.60	0.34	0.71	0.65	0.67	0.79	0.68	0.87	0.78	0.92
K	0.24	0.28	0.30	0.30	0.36	0.23	0.37	0.48	0.38	0.37	0.34	0.54	0.56	0.53
Na	0.22	0.22	0.06	0.26	0.14	0.18	0.06	0.13	0.17	0.03	0.11	0.07	0.01	–
Ca	0.15	0.14	0.15	0.15	0.12	0.15	0.11	0.13	0.12	0.13	0.13	0.11	0.07	0.09
Total	1.88	1.90	1.81	1.93	1.90	1.86	1.91	1.91	1.96	1.94	1.92	–	1.88	1.97
LO_5 semi octahedron														
Ti	2	2	2	2	2	2	2	2	2	2	2	2	2	2
$M1O_6$ octahedron														
Na	1	1	1	1	1	1	1	1	1	1	1	1	1	1
$M2O_6$ octahedron														
Na	1.44	1.41	1.44	1.35	1.43	1.44	1.49	1.30	1.41	1.50	1.42	1.39	1.33	1.42
Mn	0.09	0.08	0.10	0.09	0.08	0.07	0.09	0.10	0.08	0.10	0.09	0.06	0.05	0.04
Fe	0.47	0.51	0.56	0.56	0.49	0.49	0.42	0.60	0.51	0.40	0.49	0.45	0.61	0.47
Ca	–	–	–	–	–	–	–	–	–		–	0.1	0.01	0.07
Total	2	2	2	2	2	2	2	2	2	2	2	2	2	2
$M3O_6$ octahedron														
Ti	0.87	0.86	0.82	0.77	0.83	0.88	0.82	0.94	0.84	0.84	0.78	0.84	0.71	0.75
Mg	0.24	0.23	0.25	0.27	0.19	0.27	0.16	0.11	0.16	0.16	0.19	0.12	0.07	0.07
Fe	–	–		–	–	–	0.02				0.03	0.04	0.22	0.18
Total	1.11	1.09	1.07	1.04	1.02	1	1	1.05	1	1	1	1	1	1
SiO_4 tetrahedron														
Si	3.98	3.98	3.99	3.98	3.97	3.95	3.97	3.99	3.97	3.99	4.02	4.03	3.95	3.92
Al	0.02	0.03	0.03	0.03	0.03	0.02	0.03	0.03	0.04	0.03	0.03	0.04	0.06	0.07
Total	4	4.01	4.02	4.01	4	3.97	4	4	4	4.03	4.05	4.07	4.01	3.99
X site														
F	0.89	0.95	1.13	1.36	1.24	0.96	1.05	0.84	1.06	0.96	0.97	0.87	0.54	0.98
O	0.86	0.01	0.74	0.59	0.76	0.42	0.50	0.89	0.72	0.63	0.23	0.05	0.17	0.28
OH	0.25	1.04	0.12	0.05	–	0.62	0.45	0.27	0.22	0.42	0.80	1.08	1.29	0.74
Total	2	2	2	2	2	2	2	2	2	2	2	2	2	2

Formula coefficients calculated on the basis of 12 cations pfu. Compositions 2 correspond to lamprophyllite; 1, 3–7 fluorlamprophyllite, 8, 12, 13 – barytolamprophyllite, 9–11, 14 fruorbarytolamprophyllite. The values of the O and OH contents were obtained on the basis of the electroneutrality condition

1.2 wt.% for dyke and from 1.61 to 1.28 wt.% for Niva intrusion.. In the LGM-III from both locations the Na2O, TiO2 and MgO content decreases, whereas the Nb2O5 and K2O content increases (Table 2 and 3).

According to the modern nomenclature (Sokolova and Cámara 2017; Rastsvetaeva et al. 2016), chemical compositions of LGM from the dyke and Niva intrusion correspond to fluorlamprophyllite, fluorbarytolamprophyllite, lamprophyllite, and barytolamprophyllite (Tables 2, 3, 4 and 5).

Fluorbarytolamprophyllite, a new mineral from agpaitic syenite

Background remarks

According to the nomenclature approved by the IMA Commission on New Minerals, Nomenclature and Classification, LGM are included in the seidozerite supergroup (Sokolova and Cámara 2017). This supergroup comprises minerals whose crystal structures are based on a three-layer *HOH* module (Ferraris and Gula 2005; Rastsvetaeva and Aksenov 2011; Sokolova 2006; Belokoneva et al. 2015). The central *O* sheet of this module consists of edge-sharing *M*-centered octahedra, while the external heteropolyhedral *H* sheets are composed of Si_2O_7 diorthogroups linked by *L*-centered octahedra or "semioctahedra" in the ratio *L*: $(Si_2O_7) = 1:1$.

Sokolova and Cámara (2017) suggested to "divide the seidozerite-supergroup minerals into four groups based on the content of Ti (+ Nb + Zr + Fe^{3+} + Mg + Mn)" in the *HOH* (= TS) module (= block). This simplified approach to the nomenclature of heterophyllosilicates implies that important differences in their crystal structures are ignored. Rastsvetaeva et al. (2016) proposed the main specific features which characterize the lamprophyllite-related minerals: five-fold coordination of *L* cations in the H sheet and the absence of intermodular water molecules and/or complex anions like $(PO_4)^{3-}$, $(SO_4)^{2-}$, or $(CO_3)^{2-}$.

According to Rastsvetaeva et al. (2016), the general formula of LGM ($Z = 2$) can be written as follows: $A_2[M1M2_2M3X_2][L_2(Si_2O_7)_2O_2]$, where A = Ba, Sr, K, or Na; $M1$ = Na or Mn^{2+}; $M2$ = Na, Mn^{2+}, Fe^{2+}, or Ca; $M3$ = Ti, Mn^{2+}, Mg, Fe^{3+}, or Fe^{2+}; L = Ti or Fe^{3+}; X = OH, F, or O. The $M1$–3 and L cations have octahedral and 5-fold pyramidal

Table 4 Representative compositions of LGM from the Niva intrusion (wt.%)

	1	2	3	4	5	6	7	8	9	10	11	12	13
	crystal 1		crystal 2		crystal 3		crystal 4		crystal 5	crystal 6	crystal 7		crystal 8
	R	C	R	C	C	R	R	C	R	R	C	R	C
SiO_2	31.47	31.72	30.18	30.44	30.01	30.33	29.05	29.09	29.71	28.56	29.54	29.93	29.22
TiO_2	28.59	29.20	27.10	28.94	27.91	27.72	27.45	27.53	26.44	27.39	27.42	27.13	26.84
Al_2O_3	–	0.07	0.02	0.05	0.15	0.06	0.07	0.11	0.07	0.09	0.08	0.00	0.12
FeO	5.10	4.89	5.28	4.74	4.54	4.12	4.98	4.08	4.17	4.83	4.54	5.65	4.30
MnO	0.94	0.89	0.86	0.85	0.80	0.76	0.30	0.77	0.32	0.36	0.22	0.54	0.32
MgO	0.59	0.73	1.12	0.54	0.70	0.50	0.24	0.66	0.41	0.34	0.34	0.34	0.29
CaO	1.02	1.05	0.96	0.93	0.82	0.79	0.50	0.80	0.57	0.54	0.58	0.49	0.52
Na_2O	10.80	11.21	10.56	10.96	11.14	10.41	9.04	10.84	9.90	9.87	10.31	9.79	10.20
K_2O	2.43	2.05	1.63	2.12	1.82	2.49	3.20	2.38	2.57	2.59	2.32	2.56	2.53
BaO	10.48	7.72	9.44	8.40	10.95	12.85	17.78	13.32	19.99	17.19	16.16	16.11	18.70
SrO	7.86	10.22	10.03	10.29	9.60	7.00	4.35	8.08	3.34	5.18	6.51	5.45	5.17
ZrO_2	–	–	0.18	0.30	0.17	0.51	0.08	0.36	0.06	0.11	–	0.08	0.02
Nb_2O_5	0.09	–	–	0.22	0.35	1.12	1.61	0.60	1.08	0.14	0.30	–	1.10
Ta_2O_5	0.46	–	0.23	0.24	–	0.05	0.36	0.06	–	0.11	0.46	–	0.07
F	3.09	2.42	2.90	2.76	2.79	2.16	2.10	2.73	2.74	2.30	1.61	1.28	1.30
Total	102.92	102.17	100.49	101.78	101.75	100.87	101.11	101.41	101.37	99.60	100.39	99.35	100.70
O=F	1.30	1.02	1.22	1.16	1.17	0.91	0.88	1.15	1.15	0.97	0.68	0.54	0.55
Total*	101.62	101.15	99.27	100.62	100.58	99.96	100.23	100.26	100.22	98.63	99.71	98.81	100.15

*recalculated for the concentration of fluorine. Analysis 1–6 is LGM generation I; 7–10 - generation II; 11–13 - generation III. Zones of crystals: C – core, R – rim, I –intermediate. — below detection limit. Compositions 1–5 correspond to fluorlamprophyllite, 7,11–13 – barytolamprophyllite, 6, 8–10 – fruorbarytolamprophyllite

coordinations, respectively. The following nine mineral species belong to the lamprophyllite group: lamprophyllite, fluorlamprophyllite, barytolamprophyllite, fluorbarytolamprophyllite, lileyite, emmerichite, ericssonite, ferroericssonite, and schüllerite. Many compositional varieties of these minerals were also described. Moreover, LGM are characterized by the existence of different polytypes and syntaxial intergrowth (Rastsvetaeva et al. 2014; Belokoneva et al. 2015).

The new mineral fluorbarytolamprophyllite described below belongs to the most common structural type I (after Rastsvetaeva et al. 2016) and is the F-dominant analogue of barytolamprophyllite and the Ba-dominant analogue of fluorlamprophyllite. Monoclinic LGM belonging to the type I are listed in Table 6.

General appearance and physical properties

In both occurrences, fluorbarytolamprophyllite forms thin prismatic crystals up to 0.2 × 0.5 × 3.5 mm long, as radial aggregates up to 0.2 mm across (Figs. 3 and 4). It is also found on the rims of zoned crystals of earlier formed LGM grains. The crystals are flattened on (100) and elongate along *b*. The crystals are imperfect (represented by unshaped grains); the only observed form is {100}. Fluorlamprophyllite is brittle with the Mohs hardness of 2.5. Cleavage is perfect on {100}; parting is not observed. Fracture is uneven across the cleavage. Fluorescence is not observed. The density of fluorbarytolamprophyllite calculated using an empirical formula (see below) is 3.662 g/cm^3.

The mineral is optically biaxial (+), $\alpha = 1.738$ (3), $\beta = 1.745(4)$, $\gamma = 1.777$ (4) (589 nm), 2 *V* (meas.) = 55(5)°, 2 *V* (calc.) = 51°. Dispersion is very strong: $r > v$. The orientation is: $X = b$. The *X*- and *Z*-axes lie in the (100) plane. Under the microscope, fluorlamprophyllite is light to dark yellow. Pleochroism is distinct: *Z* (brown) > $Y \approx X$ (very pale brown to colorless).

Chemical composition

Compositional data for the fluorbarytolamprophyllite holotype specimen from the Niva intrusion are given in Table 7. The water content was determined from TGA data combined with qualitative mass-spectrometric analysis. Two stages of weight loss have been observed by thermogravimetry (Fig. 6). During the first stage (below 300 °C) a weight loss of 0.46% is observed. During the second stage (in the temperature interval from 400 to 900 °C) the weight loss is 0.28%. According to qualitative mass-spectrometric measurements, the only gaseous product evolved in both stages is H_2O. The first stage corresponds to removal of adsorbed water and

Table 5 Formula coefficients of LGM from the Niva intrusion (*apfu*)

	1	2	3	4	5	6	7	8	9	10	11	12	13
$AO_{10–11}$ polyhedron													
Sr	0.59	0.76	0.77	0.78	0.73	0.54	0.35	0.62	0.27	0.41	0.51	0.43	0.41
Ba	0.53	0.39	0.49	0.43	0.56	0.67	0.96	0.69	1.08	0.93	0.86	0.86	1
K	0.4	0.33	0.28	0.35	0.3	0.42	0.56	0.4	0.45	0.46	0.4	0.44	0.44
Na	0.25	0.33	0.31	0.3	0.31	0.12	–	0.21	–	0.15	0.1	0.12	0.03
Ca	0.14	0.14	0.14	0.13	0.12	0.11	–	0.11	0.04	0.08	0.08	0.07	0.08
Total	1.91	1.95	1.99	1.99	2.02	1.86	1.87	2.03	1.84	2.03	1.95	1.92	1.96
LO_5 semi octahedron													
Ti	2	2	2	2	2	2	2	2	2	2	2	2	2
$M1O_6$ octahedron													
Na	1	1	1	1	1	1	1	1	1	1	1	1	1
$M2O_6$ octahedron													
Na	1.46	1.44	1.4	1.46	1.52	1.57	1.42	1.58	1.63	1.49	1.6	1.46	1.66
Mn	0.10	0.10	0.10	0.09	0.09	0.09	0.04	0.09	0.04	0.04	0.03	0.06	0.04
Fe	0.44	0.46	0.5	0.45	0.39	0.34	0.47	0.33	0.29	0.47	0.37	0.48	0.3
Ca	–	–	–	–	–	–	0.07	–	0.04	–	–	–	–
Total	2	2	2	2	2	2	2	2	2	2	2	2	2
$M3O_6$ octahedron													
Ti	0.78	0.8	0.7	0.83	0.75	0.78	0.85	0.75	0.73	0.84	0.79	0.77	0.75
Mg	0.11	0.14	0.22	0.1	0.14	0.1	0.05	0.13	0.08	0.07	0.07	0.07	0.06
Fe	0.11	0.06	0.08	0.07	0.11	0.12	0.1	0.12	0.19	0.09	0.14	0.16	0.19
Total	1	1	1	1	1	1	1	1	1	1	1	1	1
SiO_4 tetrahedron													
Si	4.07	4.04	4.00	3.96	3.93	4.04	4.00	3.87	4.08	3.94	4.00	4.07	3.97
Al	0.00	0.01	0.00	0.01	0.02	0.01	0.01	0.02	0.01	0.01	0.01	0.00	0.02
Total	4	4	4	4	4	4	4	4	4	4	4	4	4
X site													
F	1.24	0.96	1.21	1.14	1.17	0.90	0.91	1.18	1.16	1.02	0.69	0.55	0.56
O	0.05	0.13	0.45	0.85	0.73	0.40	0.92	0.82	0.00	0.93	0.46	0.10	0.61
OH	0.71	0.91	0.34	0.01	0.10	0.70	0.17	0.00	0.84	0.05	0.85	1.35	0.83
Total	2	2	2	2	2	2	2	2	2	2	2	2	2

Formula coefficients calculated on the basis of 12 cations pfu. Compositions 1–5 correspond to fluorlamprophyllite, 7,11–13 – barytolamprophyllite, 6, 8–10 – fruorbarytolamprophyllite. The values of the O and OH contents were obtained on the basis of the electroneutrality condition

dehydration of impurities (zeolites *etc.*). The second stage corresponds to dehydroxylation of fluorbarytolamprophyllite.

The empirical formula of this sample calculated on the basis of 18 anions per formula unit (*apfu*) taking into account

Table 6 Cation distribution in monoclinic members of lamprophyllite group belonging to type I structure (Rastsvetaeva et al. 2016)

Mineral	Sites						References
	A	*M*1	*M*2	*M*3	*L*	*X*	
Lamprophyllite subgroup (*A* = Sr)							
Lamprophyllite-2*M*	Sr	Na	Na	Ti	Ti	OH	Krivovichev et al. 2003
Fluorlamprophyllite-2*M*	Sr	Na	Na	Ti	Ti	F	Andrade et al. 2017
Barytolamprophyllite subgroup (*A* = Ba)							
Barytolamprophyllite-2 *M*	Ba	Na	Na	Ti	Ti	OH	Rastsvetaeva and Dorfman 1995; Sokolova and Cámara 2008
Fluorbarytolamprophyllite-2*M*	Ba	Na	Na	Ti	Ti	F	This paper; Peng and Chang 1965; Peng et al. 1984; Akimenko et al. 2015
Lileyite-2*M*	Ba	Na	Na	Mg	Ti	F	Chukanov et al. 2012
Emmerichite-2*M*	Ba	Na	Na	Fe^{3+}	Ti	F	Chukanov et al. 2014; Aksenov et al. 2014
Ericssonite-2*M*	Ba	Mn^{2+}	Mn^{2+}	Mn^{2+}	Fe^{3+}	OH	Moore 1971
Ferroericssonite-2*M*	Ba	Fe^{2+}	Fe^{2+}	Fe^{2+}	Fe^{3+}	OH	Kampf et al. 2011

Table 7 Chemical composition of *holotype* fluorbarytolamprophyllite (1), *co-type* sample (2) and fluorine-rich barytolamprophyllite (3–5)

Component	(1)	(2)	(3)	(4)	(5)
SiO_2	29.35 (28.56–30.33)	28.93 (27.46–29.78)	27.87 (27.53–28.25)	29.31	28.53
TiO_2	27.31 (26.44–27.72)	27.01 (25.59–27.72)	21.83 (21.26–22.81)	28.39	26.60
Al_2O_3	0.08 (0.06–0.11)	0.26 (0.19–0.42)	–	0.16	1.12
FeO	4.44 (4.12–4.98)	4.46 (3.81–5.45)	–	2.66	2.63
Fe_2O_3	–	–	4.80 (4.57–5.08)	0.49	2.72
MnO	0.50 (0.30–0.76)	0.71 (0.35–0.89)	0.05 (0–0.35)	2.42	1.75
MgO	0.43 (0.24–0.66)	0.69 (0.35–0.92)	2.91 (2.45–3.67)	0.26	1.00
CaO	0.64 (0.50–0.79)	0.77 (0.59–0.89)	1.99 (1.62–2.40)	0.88	1.70
Na_2O	10.01 (9.04–10.84)	9.35 (8.74–9.68)	7.44 (7.23–7.69)	7.90	9.52
K_2O	2.65 (2.38–3.20)	2.36 (1.96–2.93)	2.12 (1.90–2.33)	3.52	3.10
BaO	16.23 (12.85–19.99)	14.42 (12.97–16.39)	27.32 (26.31–28.30)	16.37	17.24
SrO	5.59 (3.34–8.08)	7.33 (5.17–8.49)	–	4.11	1.47
ZrO_2	0.22 (0.11–0.51)	0.15 (0.02–0.42)	–	–	–
Nb_2O_5	0.91 (0.14–1.12)	0.79 (0.41–1.59)	–	0.11	–
Ta_2O_5	0.15 (0–0.36)	–	–	–	–
V_2O_5	–	–	0.68 (0–1.30)	–	–
F	2.41 (2.10–2.74)	2.23 (2.03–2.43)	2.70 (2.41–3.21)	1.69	1.60
Cl	–	–	–	–	0.51
H_2O	0.26*	–	–	0.77***	0.70
Total	101.18	99.46	–	–	–
–O=F	−1.01	−0.94	–	−0.71	−0.67
–O=Cl	–	–	–	–	−0.15
Total	100.17	98.52	99.71	98.33	99.4
Formula coefficients					
Si	3.98	3.98	4.04	4.00	4.00
Ti	2.79	2.80	2.38	2.91	2.81
Al	0.01	0.04	–	0.03	0.19
Fe	0.5	0.51	0.53	0.35	0.60
Mn	0.06	0.08	0.01	0.28	0.21
Mg	0.09	0.14	0.63	0.05	0.21
Ca	0.09	0.11	0.31	0.13	0.26
Na	2.63	2.49	2.09	2.09	2.59
K	0.46	0.41	0.39	0.61	0.55
Ba	0.86	0.78	1.55	0.88	0.95
Sr	0.44	0.58	–	0.33	0.12
Zr	0.01	0.01	–	–	–
Nb	0.06	0.05	–	0.01	–
Ta	0.01	–	–	–	–
V	–	–	0.07	–	–
F	1.03	0.97	1.24	0.73	0.71

Compositions: 1- Niva intrusion, 2 – agpaitic dyke; (3) P2-West "Kimberlite", Wajrakarur, Kimberlite field, Andhra Pradesh, India – Kaur and Mitchell (2013); (4) Mt. Yuksporr, Khibina alkaline massif, Kola Peninsula, Russia – Sokolova and Cámara (2008); (5) Lovozero intrusive, Kola Peninsula, Russia – Peng and Chang (1965). *From TG data; ** total Fe expressed as Fe_2O_3; ***Calculated from results of structure refinement

Samples from P2-West described by Kaur and Mitchell (2013) as "barytolamprophyllite" is chemically closer to emmerichite, because amount of Ti is less than 2.5 *apfu* and amount of Fe is more than 0.5 *apfu*. Taking into account variation in chemical composition of studied samples we can consider them as an intermediate members of fluorbarytolamprophyllite-emmerichite solid solution

structural data (see below), charge-balance requirements and general crystal-chemical constrains of LGM (Rastsvetaeva et al. 2016) is: $^{A}(Ba_{0.865}K_{0.46}Sr_{0.44}Na_{0.26})_{\Sigma 2.025}[^{M(1-2)}(Na_{2.38}Fe_{0.47}Ca_{0.09}Mn_{0.06})_{\Sigma 3.00}{}^{M(3)}(Ti_{0.875}Mg_{0.09}Fe_{0.035})_{\Sigma 1.00}$

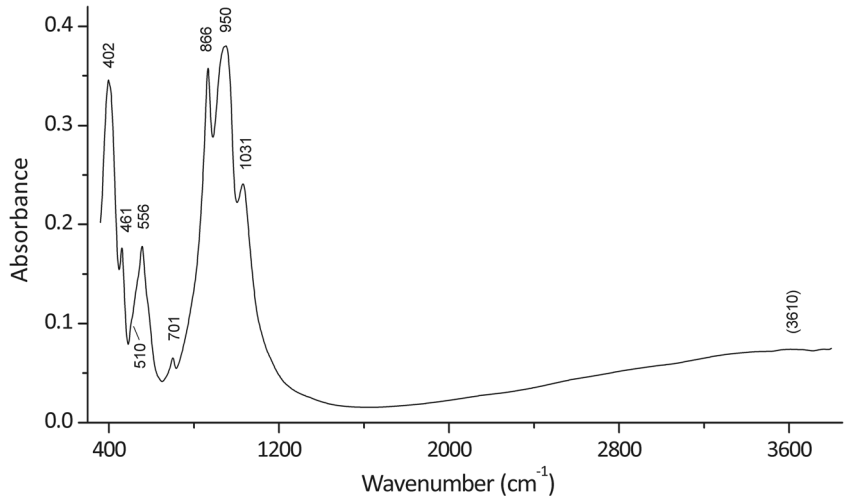

Fig. 5 IR absorption spectrum of fluorbarytolamprophyllite

$[^{L}(Ti_{1.915}Nb_{0.06}Zr_{0.015}Ta_{0.01})_{\Sigma 2.00}(Si_{3.99}Al_{0.01})_{\Sigma 4.00}O_{16}]^{X}[F1.04O_{0.72}(OH)_{0.24}]_{\Sigma 2.00}$. Magnesium is placed together with Ti because Mg substitution in the octahedral *M*3 site of LGM is well-known, up to the predominance of Mg over Ti in lileyite (Chukanov et al. 2012). The simplified formula of fluorbarytolamprophyllite is $^{A}(Ba,Sr,K)_2[^{M(1-2)}(Na,Fe^{2+})_3{}^{M(3)}Ti^{X}F_2][^{L}Ti_2(Si_2O_7)_2O_2]$.

Infrared spectroscopy

The IR spectrum of fluorbarytolamprophyllite is very close to that of barytolamprophyllite (Fig. 5) (Chukanov 2014). The bands in the range 800–1100 cm^{-1} correspond to Si–O-stretching vibrations. The range 550–630 cm^{-1} is characteristic of titanium in square-pyramidal coordination: distinct bands in this range are present in IR spectra of minerals containing TiO_5 polyhedra, namely fresnoite, natisite, paranatisite, and Ti-dominant members of the lamprophyllite group (Chukanov 2014). For this reason, the band at 556 cm^{-1} in the IR spectrum of fluorbarytolamprophyllite is assigned to Ti–O-stretching vibrations of the TiO_5 pyramid. The bands below 500 cm^{-1} correspond to lattice modes involving stretching vibrations of octahedra and bending vibrations of the Si_2O_7 diorthogroups. The weak bands at 701 and 3610 cm^{-1} may be tentatively assigned to *M*···O–H bending and O–H-stretching vibrations, respectively.

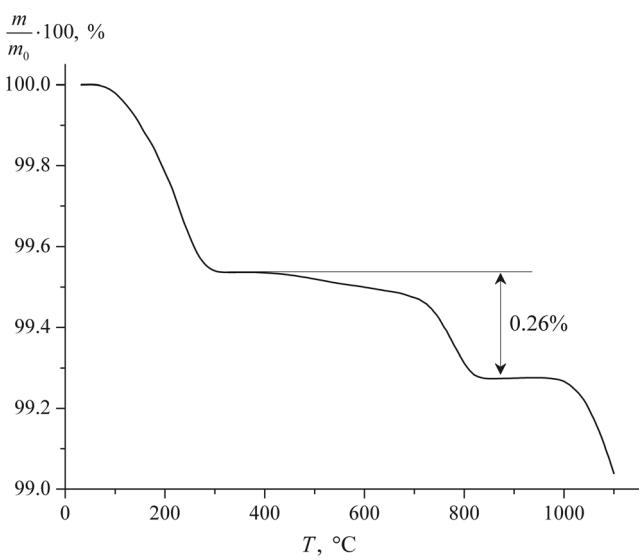

Fig. 6 TG curve for fluorbarytolamprophyllite

X-ray crystallography and crystal structure

Powder X-ray diffraction data for the holotype fluorbarytolamprophyllite sample are given in Table 8. Unit-cell parameters of the monoclinic unit cell calculated from the powder XRD data using whole pattern fitting are: a = 19.520(5) Å, b = 7.0995(17) Å, c = 5.3896(20) Å, β = 96.657(23)°, V = 741.86(24) Å^3. The following monoclinic unit-cell parameters have been obtained based on single crystal X-ray data: a = 19.538(1) Å, b = 7.092(1) Å, c = 5.391(2) Å, β = 96.704(8)°, V = 741.8(3) Å^3.

The structure determination and refinement were carried out using the Jana 2006 program package (Petříček et al. 2006). The initial model for the fluorbarytolamprophyllite structure refinement was based on the atomic coordinates of emmerichite (Aksenov et al. 2014). Illustrations were produced with the JANA2006 program package in combination with the program DIAMOND (Brandenburg and Putz 2005). Atomic scattering factors for neutral atoms together with anomalous dispersion corrections were taken from International Tables for X-Ray Crystallography (Ibers and Hamilton 1974). The experimental details of the data collection and refinement results are listed in Table 9. The final refinement cycles converged with R_1 = 5.07, wR_2 = 8.10, GOF = 1.00 for 2897 reflections with $I > 2\sigma(I)$.

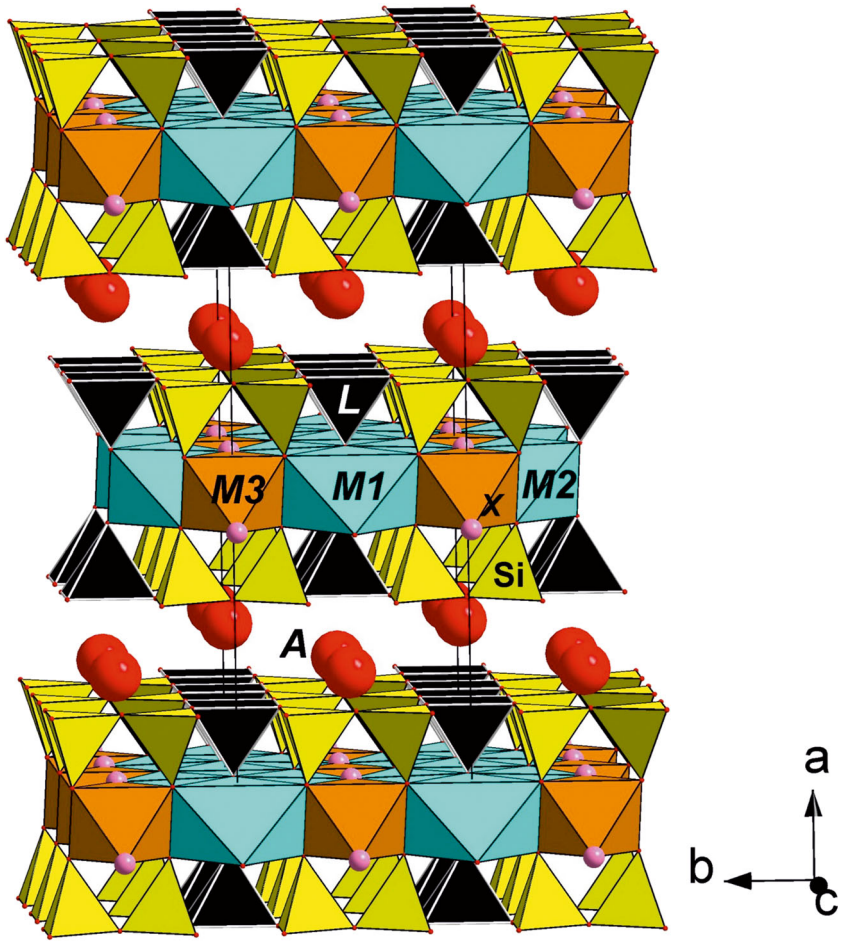

Fig. 7 General view of the fluorbarytolamprophyllite crystal structure along the c-axis

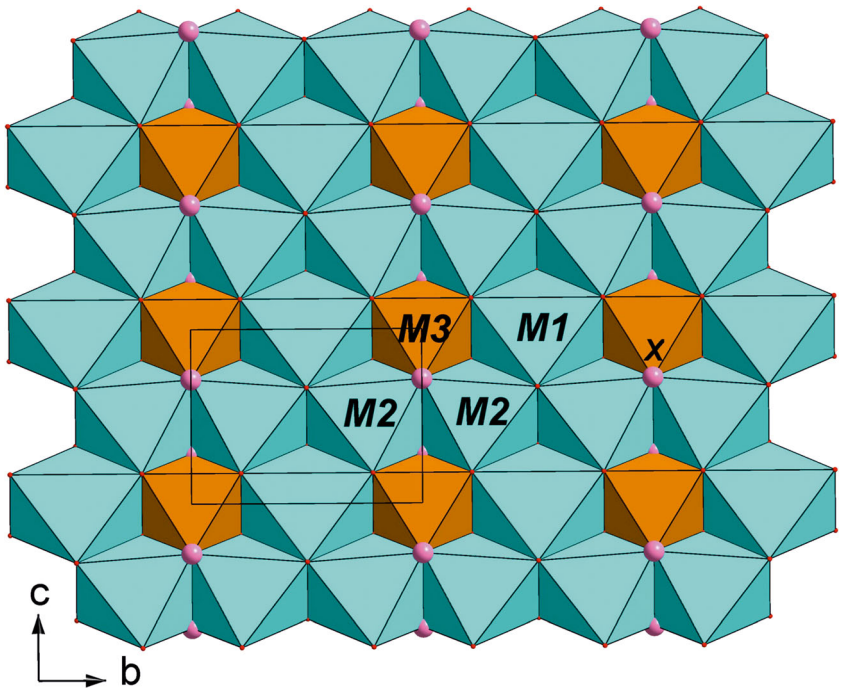

Fig. 8 *O*-sheet in fluorbarytolamprophyllite crystal structure projected on (100)

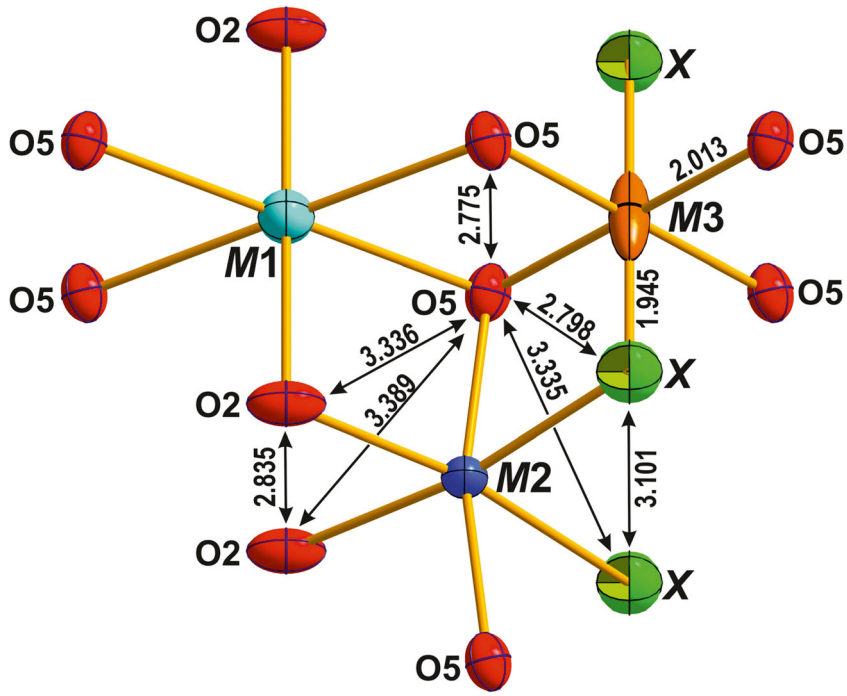

Fig. 9 Distortion of the octahedral *M*-sites in the structure of fluorbarytolamprophyllite

Table 10 lists the fractional atomic coordinates, occupancy, site symmetry and equivalent atomic displacement parameters (U_{eq}). Anisotropic atomic displacement parameters (U_{ij}) are presented in Table S1 (Supplementary Information). Selected interatomic distances and angles are given in Table 11. Bond-valence sum (BVS) calculations can be used to verify the presence of a mixed oxygen/hydroxyl/fluorine site in the structure. BVS calculations (Table 12) were performed using the bond-valence parameters for the Ca^{2+}–O, Na^{+}–O, Mg^{2+}–O, Fe^{2+}–O, Fe^{3+}–O, Al^{3+}–O, Ti^{4+}–O, and Si^{4+}–O from Brown and Altermatt (1985).

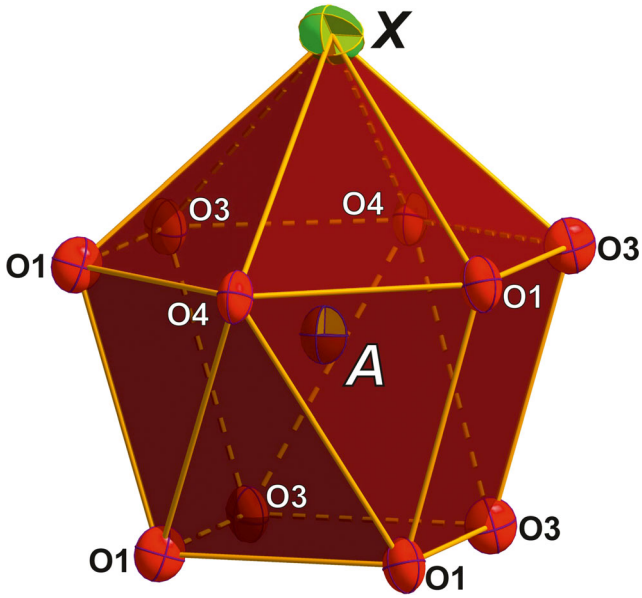

Fig. 10 Local coordination environment of the *A*-site in the structure of fluorbarytolamprophyllite

The refined crystal-chemical formula of fluorbarytolamprophyllite is ($Z = 2$): $^{A}(Ba_{0.43}K_{0.23}Sr_{0.22}Na_{0.12})_2[^{M1}Na^{M2}(Na_{0.69}Fe^{2+}_{0.235}Ca_{0.045}Mn_{0.03})_2{}^{M3}(Ti_{0.87}Mg_{0.09}Fe^{2+}_{0.04})^{X}(F_{0.52}O_{0.37}(OH)_{0.11})_2][(Ti_{0.96}Nb_{0.04})_2(Si_2O_7)_2O_2]$, where square brackets separate the compositions of the *O* and *H* sheets. The crystal structure of fluorbarytolamprophyllite is similar to those of other members of the lamprophyllite group with type 1 structures (2 *M*-polytypes) (Rastsvetaeva et al. 2016) and is based on the triple layered *HOH*-modules (Ferraris et al. 1996) (Fig. 7). The *O* sheet contains edge-shared $M(1–3)Ø_6$-octahedra (Fig. 8). The smallest $M3Ø_6$-octahedron (<*M*3–Ø> = 1.990 Å) is occupied predominantly by Ti (0.87 *apfu*) with minor amounts of Mg (0.09 *apfu*) and Fe (0.04 *apfu*). The $M2Ø_6$-octahedron (<*M*2–Ø> = 2.289 Å) is occupied by Na (1.38 *apfu*), Fe^{2+} (0.47 *apfu*), Ca (0.09 *apfu*) and Mn (0.06 *apfu*). The largest $M1O_6$-octahedron (<*M*1–O> = 2.428 Å) is fully occupied by Na. Incorporation of small cations (*i.e.* Ti^{4+}, Fe^{3+}, Mg^{2+}) in the *O*-sheet leads to distortion of octahedral sites ($\Delta^{M1} = 20.46$; $\Delta^{M2} = 2.817$; $\Delta^{M3} = 2.594$, Brown and Shannon 1973). All *M*(1–3)-polyhedra are characterized by a shorter distance to their apical vertices relative to the equatorial ones. Moreover, in the structures of LGM, the *X*–*X* distance ($X = (OH)^{-}, F^{-}$) is considerably larger than corresponding O–O distances (Fig. 9). The *H*-sheets are built by $[Si_2O_7]$ diorthogroups and isolated *L*-semioctahedra predominantly occupied by Ti (1.92 *apfu*) with minor Nb (0.08 *apfu*).

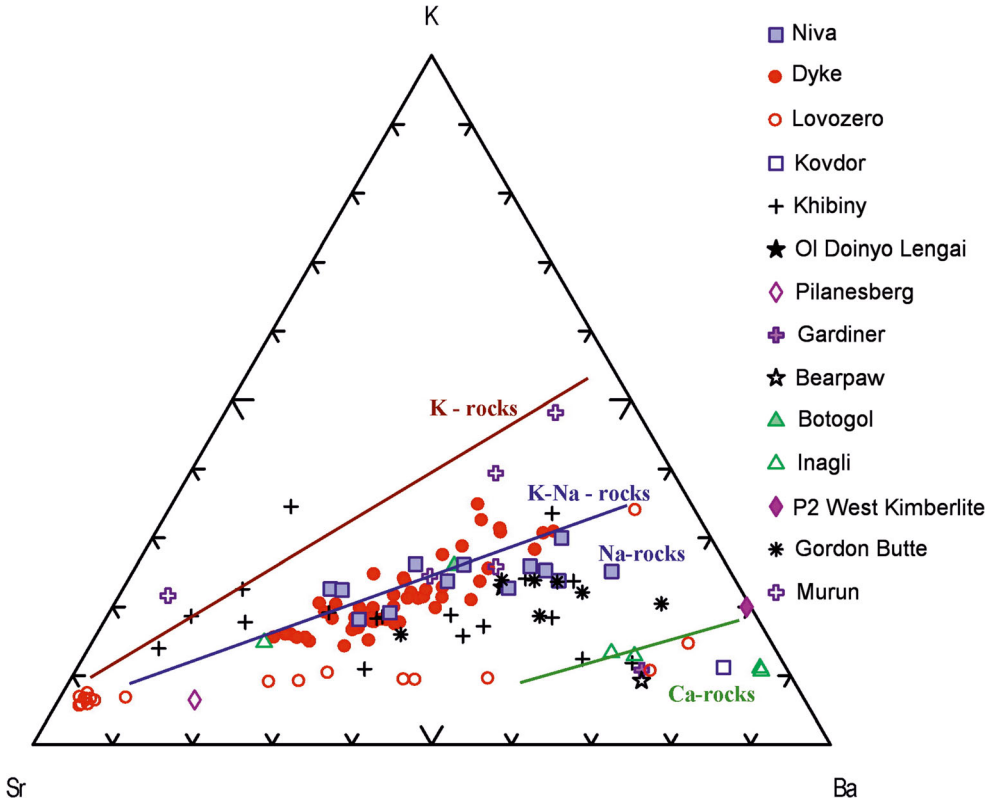

Fig. 11 Composition variation of the *A*-site cations (*apfu*) of LGM from different rocks of carbonatite and alkaline massifs, illustrating the main trend of compositional evolution towards enrichment of barium. Lines separate the composition fields of LGM from rocks enriched in alkali metals in different degree. Previous data sources: Lovozero (Zaitsev and Kogarko 2002), Khibiny (Azarova 2004), Kovdor (Ivanyuk et al. 2002), Inagli (Labeznik et al. 1998; Chukanov et al. 2004), Botogol (Kapustin 1973), Gardiner (Johnsen et al. 1994), Pilanesberg (Zaitsev and Kogarko 2002), Bearpaw (Chakhmouradian and Mitchell 1999), Ol Doinyo Lengai (Dawson 1998), P2-West Kimberlite (Kaur and Mitchell 2013), Gordon Butte (Chakhmouradian and Mitchell 2002), Murun (Konev et al. 1996)

Large cations (Ba^{2+}, Sr^{2+}, K^+, Na^+) fill the interlayer space between adjacent *HOH*-modules. Sokolova and Cámara (2016) reported that in Ba-dominant members of heterophyllosilicates belonging to Group III, typical coordination of *A*-sites varies from nine to eleven with $X^{O}{}_{A}$-anion distances of 3.15–3.79 Å. The mean *A*–φ (where φ = O, OH/F) distance ranges from 2.82 to 2.94 Å. In fluorbarytolamprophyllite, the *A*-site is coordinated by 11 anions (Fig. 10) with distances <*A*–φ> = 2.824 Å and *A*–*X* = 3.108(3) Å. The dependence of unit-cell parameters on the type of large cation in the interlayer space was reported in detail by Zaitsev (2005).

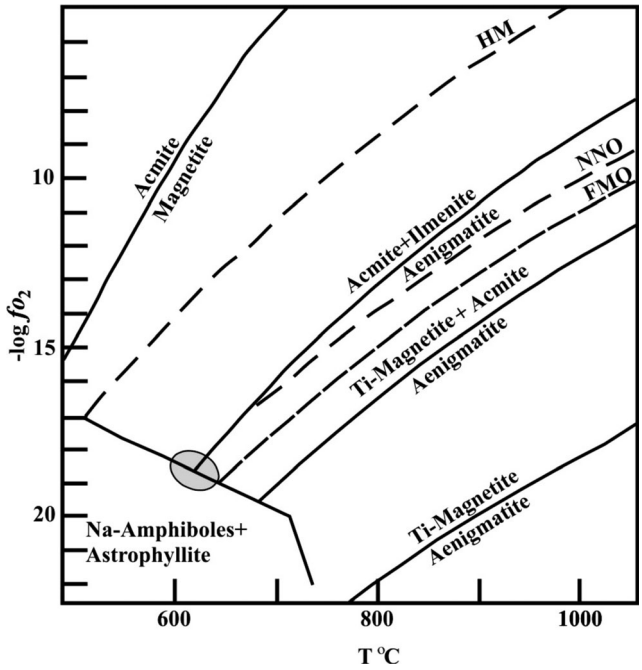

Fig. 12 Stability curves for iron-containing phases in alkaline paragenesis in terms of oxygen fugacity and temperature at 1 bar total pressure (March 1975). The shaded area represents the variation limits of T °C and fO_2 from of crystallization of early mineral association from Niva and Mokhnatye Roga alkaline dyke

The most notable crystal-chemical feature of fluorbarytolamprophyllite is the predominance of fluorine (1.04 *apfu*) over oxygen (0.74 *apfu*) and hydroxyl groups (0.22 *apfu*) in the anionic *X*-site of the *O* sheet. The predominance of F in the *X*-site is confirmed by EMPA and TG analysis. The mean average cation-anion distances in the structure of fluorbarytolamprophyllite (excluding *A*-site) are close to those in the structure of fluorlamprophyllite (Andrade et al. 2017).

Discussion

The most common LGM are characterized by the predominance of OH group over F and O in the anionic *X* position. A number of fluorine-dominant members of this family were recently discovered in the alkaline basalts of the Eifel paleovolcanic region, Germany: lileyite $Ba_2[(Na,Fe,Ca)_3MgF_2][Ti_2(Si_2O_7)_2O_2]$ (Chukanov et al. 2012), emmerichite $Ba_2[Na_3Fe^{3+}F_2][Ti_2(Si_2O_7)_2O_2]$

Table 8 Powder X-ray diffraction data (d in Å) for fluorbarytolamprophyllite

d_{obs}	I_{obs}	d_{calc*}	I_{calc*}	*hkl*
9.692	40	9.702	100	200
6.664	14	6.661	11	110
5.385	5	5.354	1	001
4.776	8	4.779	1	310
4.468	3	4.472	8	201
4.253	8	4.257	5	−111
4.096	15	4.094	38	111
3.929	4	–	–	–
3.818	8	3.824	12	−401
3.726	59	3.729	58	−311
3.549	8	3.546	20	020
3.414	67	3.422; 3.404; 3.403	44; 40; 8	311; 510; 401
3.332	15	3.330	19	220
3.230	96	3.234	22	600
3.013	53	3.016	36	−5-11
2.918	19	2.923	14	−601
2.879	32	2.880	25	−221
2.862	25	2.863	25	420
2.780	100	2.778	87	221
2.748	40	2.748	26	511
2.662	52	2.677	18	002
2.652	39	2.662	35	−202
2.642	28	2.635	17	601
2.596	30	2.600	28	−4-21
2.582	34	2.582	35	710
2.467	18	2.469	2	−402
2.459	18	2.450	3	112
2.427	11	2.431; 2.427; 2.426	4; 5; 1	−7-11; −312; 800
2.393	5	2.390	3	620
2.311	9	2.313	11	−801
2.255	12	2.256; 2.254	1; 12	−6-21; 312
2.219	13	2.220; 2.218	5; 10	330; −512

*Calculated from structural data. Peaks with d below 2.20 Å could not be assigned unambiguously because of multiple, relatively weak overlapping reflections

Table 9 Crystal parameters, data collection and structure refinement details for fluorlamprophyllite

Crystal data	
Formula	
Formula weight (g)	819.8
Temperature (K)	293
Cell setting	Monoclinic
Space group	*C*2/*m*
a (Å)	19.538(1)
b (Å)	7.092(1)
c (Å)	5.391(2)
β (°)	96.704(8)
V (Å^3)	741.8(3)
Z	2
Calculated density, D_x (g cm^{-3})	3.669
Crystal size (mm)	0.12 × 0.15 × 0.15
Crystal form	Anhedral grain
Data collection	
Diffractometer	Bruker Smart Apex II
Radiation; λ	MoK_α; 0.71073
Absorption coefficient, μ (mm^{-1})	6.54
F (000)	773
Data range θ (°); h, k, l	3.06–47.32; $-40 < h < 40$, $-14 < k < 14$, $-11 < l < 11$
No. of measured reflections	42,475
No. total (N_2) / unique (N_1) reflections	3364 / 2897
Criterion for observed reflections	$I > 2\sigma(I)$
R_{int} / R_σ, (%)	5.83 / 2.63
Refinement	
Refinement onye	Full-matrix least squares on F
Weight scheme	$1/(\sigma^2\lvert F\rvert + 0.004225F^2)$
R_1 / wR_1, (%)	5.07 / 5.96
R_2 / wR_2, (%)	7.57 / 8.10
GOF (Goodness of fit)	1.00
Max./min. Residual e density, (eÅ^{-3})	−2.46 / 2.50*

$R_1 = \sum(|F_{obs}| - |F_{calc}|) / \sum|F_{obs}|$; $wR_2 = \{\sum[w(F_{obs}^2 - F_{calc}^2)^2] / \sum[w(F_{obs}^2)^2]\}^{1/2}$;

GOF = $\{\sum[w(F_{obs}^2 - F_{calc}^2)] / (n-p)\}^{1/2}$ where n is a number of reflections and p is a number of refined parameters

* The rather big final values of $\Delta\rho_{min}$ and $\Delta\rho_{max}$ could be explain by inhomogeneous chemical composition and bad quality of the crystals

(Aksenov et al. 2014; Chukanov et al. 2014), and schüllerite $Ba_2[NaMnFe^{2+}Fe^{3+}F_2][Ti_2(Si_2O_7)_2O_2]$ (Rastsvetaeva et al. 2011; Chukanov et al. 2011). Fluorlamprophyllite $(Sr,Na)_2[(Na,Mn)_3(Ti,Fe)(F,OH)_2][Ti_2(Si_2O_7)_2O_2]$, the F-dominant analogue of lamprophyllite, was discovered in the Poços de Caldas alkaline massif, Brazil (Andrade et al. 2017). Comparative data for these minerals are given in Table 13.

Barytolamprophyllite varieties with high fluorine contents (F > OH, O) have been described from various localities. Peng and Chang (1965) discovered barytolamprophyllite with 0.71 *apfu* F in ijolite of the Lovozero intrusive, Kola Peninsula, Russia. Sokolova and Cámara (2008) studied a sample of fluorine-rich barytolamprophyllite (with 0.73 *apfu* F) from Mt. Yuksporr, Khibiny alkaline massif, Kola Peninsula, Russia. A F- and Ba-dominant LGM (with F contents in the range from 2.41 to 3.21 wt.%) has been recently described by Kaur and Mitchell (2013) in Ca-rich pegmatite rocks of P2-West "Kimberlite", Wajarakarur kimberlite field, Andhra Pradesh, India, where it occurs as a late-stage residual phase in a pegmatitic facies. Samples from P2-West "Kimberlite" described by these authors as barytolamprophyllite are

Table 10 Fractional site coordinates, site multiplicities (Q), equivalent displacement parameters (U_{eq}, Å^2) and site composition for fluorbarytolamprophyllite

Site	x	Y	z	Q	U_{eq}	Site occupancy
A	0.2838(1)	0	0.2628(1)	4	0.0172(1)	$Ba_{0.43}K_{0.23}Sr_{0.22}Na_{0.12}$
*M*1	0.5	0.5	0	2	0.0213(5)	Na
*M*2	0	0.2598(1)	0.5	4	0.0153(2)	$Na_{0.69}Fe^{2+}_{0.235}Ca_{0.045}Mn_{0.03}$
*M*3	0	0.5	0	2	0.0340(3)	$Ti_{0.87}Mg_{0.09}Fe^{2+}_{0.04}$
Si	0.3582(1)	0.7842(1)	0.7959(1)	8	0.0108(1)	Si
L	0.3515(1)	0.5	0.2935(1)	4	0.0108(1)	$Ti_{0.96}Nb_{0.04}$
O1	0.3269(1)	0.6884(2)	0.5348(3)	8	0.0157(3)	O
O2	0.4384(1)	0.5	0.3326(5)	4	0.0233(6)	O
O3	0.3264(1)	0.3121(2)	0.0297(3)	8	0.0158(3)	O
O4	0.3251(1)	1	0.7812(4)	4	0.0135(3)	O
O5	0.4412(1)	0.7943(2)	0.8289(3)	8	0.0168(3)	O
X	0.4433(2)	0	0.2735(6)	4	0.0266(6)	$F_{0.52}O_{0.37}(OH)_{0.11}$

U_{eq} is defined as one third of the trace of the orthogonalized U_{ij} tensor

chemically closer to emmerichite than to fluorbarytolamprophyllite because the amount of Ti is less than 2.5 *apfu* and the amount of Fe is more than 0.5 *apfu* (Table 7). Taking into account variation in chemical composition, as well as high contents of Mg, we can consider samples from P2-West "Kimberlite" as intermediate members of the fluorbarytolamprophyllite-emmerichite-lileyite solid-solution system (Table 3). LGM of similar composition occur also in pneumatolytic associations related to alkaline besalt of the Auf'm Kopp Mountain, Eifel, Germany (our unpublished data). It is to be noted that Ba-dominant LGM occur not only in peralkaline potassic rocks (Chakhmouradian and Mitchell 1999, 2002) but also in associations related to potassic-sodium-, sodium- and calcium-enriched rocks.

Table 11 Selected bond lengths (Å) and angles for fluorbarytolamprophyllite

Bond		Distance
A	O3	2.723(2) × 2
	O1	2.730(2) × 2
	O4	2.807(2)
	O4	2.817(2)
	O3	2.848(2) × 2
	O1	2.865(2) × 2
	X	3.108(3)
Mean		2.824
L	O2	1.687(3)
	O1	1.963(2) × 2
	O3	1.969(2) × 2
Mean		1.910
Si	O5	1.612(1)
	O1	1.617(1)
	O3	1.619(1)
	O4	1.660(1)
Mean		1.627
*M*1	O2	2.273(3) × 2
	O5	2.506(1) × 4
Mean		2.428
*M*2	O5	2.236(2) × 2
	X	2.307(2) × 2
	O2	2.325(2) × 2
Mean		2.289
*M*3	*X*	1.945(3) × 2
	O5	2.013(1) × 4
Mean		1.990
Angle		°
O1–Si–O3		110.10(9)
O1–Si–O4		103.88(9)
O1–Si–O5		112.83(9)
O3–Si–O4		104.07(9)
O3–Si–O5		113.90(9)
O4–Si–O5		110.22(9)

Agpaitic syenites of the Niva intrusion and the Mokhnatye Roga alkaline dyke are unique rocks in which LGM enriched in barium and fluorine are not accessory, but are significant rock-forming minerals. Several generations of LGM formed in agpaitic syenites of the Niva intrusion and the Mokhnatye Roga dyke during all stages of rock formation from a melt enriched in alkalis, Sr, Ba, F, Si, Ti and Nb. LGM-I corresponds to lamprophyllite, fluorlamprophyllite and fluorbarytolamprophyllite, LGM-II is represented by barytolamprophyllite and fluorbarytolamprophyllite, and the composition of LGM-III minerals ranges from barytolamprophyllite to fluorbarytolamprophyllite (Tables 2, 3 and 4).

The early generations are characterized by growth zoning, which manifests itself as an increase in the Ba and, sometimes, K contents. Positive Ba–K and Sr–Na correlations and negative Ba–Sr, Ba–Mg and Sr–K correlations have been established (Akimenko et al. 2015). The Ba–Mg correlation may be explained by a decrease in Mg concentrations in the melt during the crystallization of LGM, due to co-crystallization of Mg-bearing pyroxenes, amphiboles and aenigmatite. Most of the element correlations reflect isomorphic substitutions among *A* cations. Other correlations between Na, Ti, Fe, Mg, and Mn could be explained by complex substitutions in the octahedral *O* sheet, according to the scheme of heterovalent isomorphism proposed by

Table 12 Bond valence balance in fluorbarytolamprophyllite

Site	*A*	*L*	*M*1	*M*2	*M*3	Si	V_a
O1	$(0.23+0.16)_{\times 2\downarrow}$	$0.67_{\times 2\downarrow}$				1.02	2.08
O2		1.41	$0.28_{\times 2\downarrow}$	$0.25_{\times 2\downarrow}$			1.94
O3	$(0.23+0.16)_{\times 2\downarrow}$	$0.66_{\times 2\downarrow}$				1.01	2.06
O4	0.18 + 0.18					$0.91^{\times 2\rightarrow}$	2.18
O5			$0.15_{\times 4\downarrow}$	$0.30_{\times 2\downarrow}$	$0.58_{\times 4\downarrow}$	1.03	2.06
X	0.09			$0.18_{\times 2\downarrow}$	$0.60_{\times 2\downarrow}$		0.87
V_c	2.01	4.07	1.16	1.46	3.52	3.97	

BVS is obtained by multiplying on site occupancy factor (taking into account site multiplicity). In mixed sites, bond-valence contribution of each cation has been weighted according to its occupancy. The ×2↓ sign indicates the doubling of the corresponding valence contributions in columns due to symmetry

Rastsvetaeva et al. (2016): $Na^{+}+Ti^{4+}+O^{2-} \leftrightarrow (Mn,Fe)^{2+}+Mg^{2+}+(F,OH)^{-}$. The isovalent substitution in the A site may explain the observed correlation between Ba and Sr. Lamprophyllite and barytolamprophyllite form a continuous isomorphous series (Azarova 2004; Peng and Zhang 1965; Rastsvetaeva and Dorfman 1995).

A ternary diagram showing the relative proportions of K, Sr and Ba in the formula (Fig. 11) is based on chemical analyses of the LGM of all generations from the agpaitic syenites of the Niva intrusion and Mokhnatye Roga dyke, and from other localities. According to the degree of enrichment of rocks in K, Na or Ca, four hypothetical compositional fields are identified. LGM from the studied agpaitic syenite correspond to the compositional field for K-Na and Na rocks. The rocks of K-Na geochemical affinity are characterized by LGM with the widest compositional variations. Monoclinic Ti-bearing LGM form a continuous solid-solution series (Azarova 2004; Peng and Chang 1965; Rastsvetaeva et al. 1995). Figure 11 illustrates the main trend from low-Ba to high-Ba compositions during the evolution of the agpaitic dyke and Niva intrusion: enrichment in Ba is accompanied by enrichment in K, with constant high content of F. LGM from the Lovozero massif (differentiated and eudialyte complexes, porphyry lujaurites: Zaitsev and Kogarko 2002), the Pilanesberg (Zaitsev and Kogarko 2002) and the Inagli massifs (Labeznik et al. 1998, Chukanov et al. 2004) have lower potassium contents. Samples from the Lovozero and Khibiny massifs (Azarova 2004) form a wide compositional field, partly supplementing the general trend from strontium- to barium-rich species. The composition with the highest Ba content is barytolamprophyllite from the Kovdor carbonatite massif (26.4 wt.% BaO at no detectable Sr) (Ivanyuk et al. 2002). The composition with the highest Sr content (17.1 wt.% SrO) and 5.7 wt.% BaO was reported from the Pilanesberg alkaline massif (Zaitsev and Kogarko 2002).

All generations of LGM from the Niva intrusion and Mokhnatye Roga dyke are characterized by high Ba and F contents, due to high amounts of Ba and high F activity in the initial alkaline melts. As noted above, later LGM generations have higher K and lower Na contents compared to the earlier LGM generations. The decrease in Na contents may be explained by co-crystallization of LGM-III with Na-rich minerals such as natrolite and astrophillite. Large amount of natrolite and astrophyllite crystalized in the rocks during the hydrothermal stages. The later generations of LGM are characterized a stable content of niobium up to 1.5 wt.%. Taking into account that the LGM are rock-forming minerals associated with niobium-enriched rutile and shchervbakovite (containing up to 2.33 and 3.51 wt.% Nb_2O_5, respectively), one may suggest that the activity of Nb increases during late stages of formation of agpaitic syenites.

The compositions of pyroxene and amphibole minerals suggest that the agpaitic syenites of the Niva intrusion and the dyke evolved towards enrichment in Na, K, Fe, and F. Aenigmatite may form as a result of reaction between a Ti-rich magnetite and a peralkaline silica-undersaturated melt (March 1975). Textural relations between the minerals of the agpaitic syenites indicate an early crystallization of aegirine, ilmenite, and aenigmatite. According to the phase diagram for Fe-bearing phases in alkaline systems (Fig. 12), ilmenite, aenigmatite and astrophyllite may coexist over a wide temperature range, from 600 to 1100 °C (March 1975). According to the conditions of zeolite crystallization at the hydrothermal stage of alkaline rock evolution, natrolite formed at temperatures ≤300 °C (Barrer 1982). The range of temperature and oxygen fugacity during crystallization are close to that of the similar types of rocks from the Ilimaussak and Khibiny massifs (Marks and Markl 2017).

The agpaitic syenite of Mokhnatye Roga and Niva are crystallized from a fluorine-rich peralkaline melt enriched in incompatible elements. The average Ba contents are: 5544 ppm in the Niva agpaitic syenite, 6093 ppm in the dyke, 1232 ppm in the average agpaitic syenite of the Khibiny, and 259 ppm at Lovozero (Arzamastsev et al. 2001). Typically, nepheline is an important rock-forming mineral of agpaitic syenites. However, this mineral was not observed in either the Niva intrusion or the dyke. The agpaitic syenite suite is SiO_2 undersaturated, with a normative nepheline content of

Table 13 Comparative data for fluorbarytolamprophyllite and some related minerals

Mineral	Fluorbarytolamprophyllite	Barytolamprophyllite	Lamprophyllite	Nabalamprophyllite
Simplified formula	$Ba_2(Na,Fe,Ca)_3$ $MgTi_2(Si_2O_7)_2$ O_2F_2	$Ba_2(Na,Fe,Mn)_3$ $Ti_3(Si_2O_7)_2$ $O_2(O,OH,F)_2$	$Sr_2(Na,Fe,Mn)_3$ $Ti_3(Si_2O_7)_2$ $O_2(O,OH,F)_2$	$Ba(Na,Ba)Na_3$ $Ti_3(Si_2O_7)_2$ $O_2(OH)_2$
Symmetry	Monoclinic, *C2/m*	Monoclinic, *C2/m*	Monoclinic, *C2/m*	Monoclinic, *P2/m*
a, Å	19.538	19.833	19.431	19.741
b, Å	7.092	7.089	7.086	7.105
c, Å	5.391	5.393	5.392	5.408
β, °	96.704	96.66	96.75	96.67
Z	2	2	2	2
Strong lines of the X-ray powder-diffraction pattern: *d*, Å (*I*, %)	9.692 (40) 3.726 (59) 3.414 (67) 3.230 (96) 3.013 (53) 2.780 (100) 2.662 (52)	3.447 (70) 3.294 (50) 2.801 (100) 2.153 (90) 1.790 (70) 1.601 (80) 1.482 (90)	3.73 (40) 3.43 (55) 3.27 (40) 2.874 (40) 2.773 (100) 2.130 (45) 1.477 (45)	9.87 (96) 3.75 (65) 3.45 (90) 3.275 (78) 3.040 (41) 2.797 (100) 2.610 (43)
Optical data:				
α	1.738	1.735–1.743	1.733–1.751	1.750
β	1.745	1.741–1.754	1.740–1.760	1.755
γ	1.777	1.767–1.778	1.769–1.781	1.799
Optical sign, 2 V	+55	+30 − +45	+21 − +43	+40
Density, g/cm^3	3.662	3.62–3.66	3.44–3.53	3.65
IR absorption bands, cm^{-1}	(3610)			3610
	1031	1035	1036	1033
	950	956	943	954
		925		921
	866	863	878	854
	701	697	705	692
	556	580	580	580
	510	552	556	549
			535	
	461	458	461	459
				420
	402	395	402	402
References	This work	Peng and Chang 1965; Peng et al. 1984; Rastsvetaeva et al. 1995; Feklichev 1989	Vlasov et al. 1966; Saf'yanov et al. 1983; Rastsvetaeva et al. 1990; Feklichev 1989	Chukanov et al. 2004

10–15%. The presence of sodic pyroxenes and amphiboles, as well as natrolite in place of nepheline are characteristic for the studied syenites. A relatively low alumina content combined with an excess of alkalis results in an extremely high peralkalinity index of 1.2–1.7. This may indicate an influx of Na_2O and K_2O, which occurred at the postmagmatic stage of the rock formation and resulted in the substitution of nepheline and primary alkaline feldspar by orthoclase and natrolite, as was previously described for the Khibiny and Lovozero alkaline massifs (Kostyleva-Labuntsova et al. 1978). Syenite of the Niva intrusion is more natrolitized than that in the dyke. The presence of natrolite in the syenite indicates increasing water activity during the rock formation.

Conclusion

The new mineral fluorbarytolamprophyllite which belongs to LGM has been described in the present paper. It belongs to the most common structural type I (after Rastsvetaeva et al. 2016) and is the F-dominant analogue of barytolamprophyllite and the Ba-dominant analogue of fluorlamprophyllite. The

discovery of fluorbarytolamprophyllite expanded the range of known LGM compositions and emphasized their role as indicators of the condition of mineral formation. An important petrological and mineralogical feature of peralkaline syenites of the Niva intrusion and Mokhnatye Roga dyke, Kola Peninsula is the presence of LGM as the main rock forming minerals constituting up to 25 vol.%. LGM crystallized later than the other main minerals during the magmatic stage (potassic feldspar, Ti-rich aegirine-augite, aenigmatite and amphiboles). LGM crystallization occurred during the magmatic and hydrothermal stages of formation of the Niva intrusion and the Mokhnatye Roga dyke.

Acknowledgements Authors thank Dr. A.R. Chakhmouradian, an anonymous reviewer for useful comments and suggestions, and Dr. Leonid Danyushevsky for handling the manuscript. This study was supported by the Russian Foundation for Basic Research (grant no. 16-35-00537-mol-a), Foundation of the President of the Russian Federation, grant No. MK-8990.2016.5 (in the part of single crystal X-ray analysis) as well as Russian Science Foundation, grant no. 14-17-00048 (in part of IR spectroscopy and thermal analysis).

References

Akimenko MI, Aksenov SM, Sorokhtina NV, Kogarko LN, Kononkova NN, Rastsvetaeva RK, Rozenberg KA (2015) Variations in the chemical composition of lamprophyllite group minerals and the crystal structure of fluorine-rich barytolamprophyllite from new peralkaline dyke. Crystallography Reports 60:821–830

Akimenko MI, Kogarko LN, Sorokhtina NV, Kononkova NN, Mamontov VP (2014) A new occurrence of alkaline magmatism on the Kola Peninsula: an agpaitic dyke in the Kandalaksha region. Dokl Earth Sci 458:1125–1128

Aksenov SM, Rastsvetaeva RK, Chukanov NV (2014) The crystal structure of emmerichite $Ba_2(Na,Mg)_3Fe^{3+}Ti_2(Si_2O_7)_2O_2F_2$, a new lamprophyllite-group mineral. Z Kristallogr 229(1):1–7

Andrade MB, Yang H, Downs RT Färber G, Contreira Filho RR, Evans SH, Loehn CW, Schumer BN (2017) Fluorlamprophyllite, $Na_3(SrNa)Ti_3(Si_2O_7)_2O_2F_2$, a new mineral from Poços de Caldas alkaline massif, Morro do Serrote, Minas Gerais, Brazil. Mineral Mag 2017. https://doi.org/10.1180/minmag.2017.081.027

Arzamastsev AA, Bea F, Glaznev VN, Arzamastseva LV, Montero P (2001) Kola alkaline province in the Paleozoic: an estimate of the composition of the primary mantle melts and magmogenesis conditions. Ros Zhurn Nauk O Zemle 3(1):1–35

Arzamastsev AA, Belyatskiy BV, Arzamastseva LV (2000) Agpaitic magmatism in the northeastern Baltic Shield: a study of the Niva intrusion, Kola Peninsula, Russia. Lithos 51:27–46

Arzamastsev AA, Chashchin VV, Arzamastseva LV (1999) The Niva Pluton: a new occurrence of the agpaitic magmatism in the Kola alkaline province. Doklady Earth Sci Sect 365(3):305–308

Arzamastsev AA, Fedorov ZA, Arzamastseva LV (2009) Dyke magmatism of the north-eastern part of the Baltic Shield. Nauka, St. Petersburg, 383 pp

Azarova YV (2004) Genesis and minerals typochemistry of number lamprophyllite-barytolamprophyllite from the lujaurite-malignite complex of Khibiny massif. New Data on Minerals 39: 66–72 (in Russian)

Barrer RM (1982) Hydrothermal Chemistry of Zeolites. Academic Press, London, 420 pp

Belokoneva EL, Topnikova AP, Aksenov SM (2015) Topolology-symmetry law of structure of natural titanosilicate micas and related heterophyllosilicates based on the extended OD theory: structure prediction. Crystallogr Rep 60(1):1–15

Brandenburg K, Putz H (2005) DIAMOND Version 3. Crystal Impact GbR, Bonn

Brown ID, Altermatt D (1985) Bond-valence parameters obtained from a systematic analysis of the inorganic crystal structure database. Acta Cryst 41:244–247

Brown ID, Shannon RD (1973) Empirical bond strength–bond lengths curves for oxides. Acta Cryst 29:266–282

Chakhmouradian AR, Mitchell RH (1999) Primary, agpaitic and deutric stages in the evolution of accessory Sr, REE, Ba and Nb-mineralization in nepheline-syenite pegmatites at pegmatite peak, Bearpaw Mts, Montana. Mineral Petrol 67:85–110

Chakhmouradian AR, Mitchell RH (2002) The mineralogy of Ba- and Zr-rich alkaline pegmatites from Gordon Butte, Crazy mountains (Montana, USA): comparisons between potassic and sodic agpaitic pegmatites. Contrib Mineral Petrol 143:93–114

Chukanov NV (2014) Infrared Spectra of Mineral Species: Extended Library. Springer-Verlag GmbH, Dordrecht–Heidelberg–New York–London 1716

Chukanov NV, Moiseev MM, Pekov IV, Lazebnik KA, Rastsvetaeva RK, Zayakina NV, Ferraris G, Ivaldi G (2004) Nabalamprophyllite $Ba(Na,Ba)\{Na_3Ti[Ti_2O_2Si_4O_{14}](OH,F)_2\}$, a new layered lamprophyllite-group mineral from the alkaline-ultrabasicmassifs Inagli and Kovdor, Russia. Zapiski Vserossiiskogo Mineralogicheskogo Obshchestva 133(1):59–72 (in Russian)

Chukanov NV, Pekov IV, Rastsvetaeva RK, Aksenov SM, Zadov AE, Van KV, Blass G, Schüller W, Ternes B (2012) Lileyite, Ba2(Na,Fe, Ca)3MgTi2(Si2O7)2O2F2, a new lamprophyllite group mineral from the Eifel volcanic area, Germany. Eur J Mineral 24(1):181–188

Chukanov NV, Rastsvetaeva RK, Aksenov SM, Blass G, Pekov IV, Belakovskiy DI, Tschörtner J, Schüller W, Ternes B (2014): Emmerichite, $Ba_2Na(Na,Fe^{2+})_2(Fe^{3+},Mg)Ti_2(Si_2O_7)_2O_2F_2$, a new lamprophyllite-group mineral from the Eifel paleovolcanic region, Germany. New Data on Minerals 49:5 G 13 (in Russian)

Chukanov NV, Rastsvetaeva RK, Britvin SN, Virus AA, Belakovskiy DI, Pekov IV, Aksenov SM, Ternes B (2011) Schüllerite, $Ba_2Na(Mn,Ca)(Fe^{3+},Mg,Fe^{2+})_2Ti_2(Si_2O_7)_2(O,F)_4$, a new mineral species from the Eifel volcanic district, Germany. Geology of Ore Deposits 53: 767–774

Daly JS, Balagansky VV, Timmerman MJ, Whitehouse MJ (2012) The Lapland-Kola orogen: Palaeoproterozoic collision and accretion of the northern Fennoscandian. In book: European Lithosphere Dynamics, Chapter: Lapland-Kola orogen: Palaeoproterozoic collision and accretion of the northern Fennoscandian lithosphere. Publisher: Geological Society of London, 579–597

Dawson JB (1998) Peralkaline nephelinite-natrocarbonatite relationships at Ol Doinyo Lengai, Tanzania. J Petrol 39:2077–2094

Ernst RE, Bell K (2010) Large igneous provinces (LIPs) and carbonatites. Mineral Petrol 98:55–76

Feklichev VG (1989) Diagnostic Constants of Minerals. Nedra, Moscow (in Russian)

Ferraris G, Ivaldi G, Khomyakov AP, Soboleva SV, Belluso E, Pavese A (1996) Nafertisite, a layered titanosilicate member of a polysomatic series including mica. Eur J Mineral 8:241–249

Ferraris G, Gula A (2005) Polysomatic aspects of microporous minerals - Heterophyllosilicates, palysepioles and rhodesite-related structures. In G. Ferraris and S. Merlino (Eds.). Micro- and Mesoporous Mineral Phases. Rev Mineral Geochem 57:69–104

Gerasimovskii VI, Volkov VP, Kogarko LN, Polyakov AI, Saprykina TV, Balashov YA (1966) Geochemistry of the Lovozero alkaline massif, Moscow, 394 pp (in Russian)

Haggerty SE, Anthony NM (1983) Strontian-loparite and strontio-chevkinite: Two new minerals in rheomorphic fenites from the

Paraná Basin carbonatites, South America. Contrib Mineral Petrol 84:365–381

Ibers JA, Hamilton WC (1974) International tables for X-ray crystallography. Vol. IV. The Kynoch Press, Birmingham

Ivanyuk GY, Yakovenchuk VN, Pakhomovskii YA (2002) Kovdor. Laplandia Minerals. Apatity, 326 pp (in Russian)

Johnsen O, Nielsen TFD, Ronsbo JG (1994) Lamprophyllite and barytolamprophyllitefrom the Tertiary Gardiner complex, East Greenland. Neues Jahrbuch für mineralogie 7:328–336

Kampf AR, Roberts AC, Venance KE, Dunning GE, Walstrom RE (2011) Ferroericssonite, the Fe^{2+} analogue of ericssonite, from Eastern Fresno County, California, U.S.A. Can Mineral 49:587–594

Kapustin YL (1973) About the new findings of barytolamprophyllite and the chemical formula of lamprophyllite. Reports of the Academy of Sciences 210:921–924 (in Russian)

Kaur G, Mitchell RH (2013) Mineralogy of the P2-West "Kimberlite", Wajrakarur kimberlite field, Andhra Pradesh, India: kimberlite or lamproite. Mineral Mag 77(8):3175–3196

Kogarko LN, Lahaye Y, Brey G, Foulger PGR, Jurdy DM (2009) Plume-related mantle source of super-large rare metal deposits from the Lovozero and Khibina massifs on the Kola Peninsula, Eastern part of Baltic Shield: Sr, Nd and Hf isotope systematics Plates, Plumes, and Planetary Processes. The Geological Society of America. Special Paper 430–999

Konev AA, Vorobyev EI, Labeznik KA (1996) Mineralogy of the Murun alkaline massif. Publishing house of the Siberian Branch of the Russian Acad. Sci., Novosibirsk, 222 pp (in Russian)

Kostyleva-Labuntsova EE, Borutsky BE, Sokolova MN, Shlyukova Z, Dorfman MD, Dudkin OB, Kozyreva LV (1978) Mineralogy of the Khibiny Massif. Nauka, Moscow, pp 228–586 (in Russian)

Krivovichev SV, Armbruster T, Yakovenchuk VN, Pakhomovsky YA, Men'shikov YP (2003) Crystal structures of lamprophyllite-2M and lamprophyllite-2O from the Lovozero alkaline massif, Kola peninsula, Russia. Eur J Mineral 15:711–718

Kukharenko AA, Orlova MP, Bulakh AG (1965) The Caledonian Complex of ultrabasic, alkaline rocks, and carbonatites of Kola Peninsula and Northern Karelia, vol 772. Nedra, Moscow (in Russian)

Labeznik KA, Zayakina HB, Paukevich HS (1998) Without strontium lamprophyllite - a new member of the lamprophyllite group. Reports of the Academy of Sciences 361:799–802 (in Russian)

March JS (1975) Aenigmatite stability in silica-undersaturated rocks. Contrib Mineral Petrol 50:135–144

Moiseev MM, Chukanov NV (2006) Mineralogy of alkaline pegmatites and hydrothermalites of the Kovdor massif. New Data on Minerals 41:56–70

Marks MAW, Markl G (2017) A global review on agpaitic rocks. Earth Sci Rev 173:229–258

Moore PB (1971) Ericssonite and orthoericssonite. Two new members of the lamprophyllite group from Långban, Sweden. Lithos 4:137–145

Peng TC, Chang CH (1965) New varieties of lamprophyllite–barytolamprophyllite and orthorhombic lamprophyllite. Sci Sinica 14(12):1827–1840

Peng Z, Zhang J, Shu J (1984) The crystal structure of barytolamprophyllite. Kexue Tongbao 29:237–241

Petříček V, Dušek M, Palatinus L (2006) Jana2006: Structure determination software programs. Institute of Physics, Praha

Rastsvetaeva RK, Aksenov SM (2011) Crystal Chemistry of Silicates with Three-Layer TOT and HOH Modules of Layered, Chainlike, and Mixed Types. Crystallogr Rep 56(6):910–934

Rastsvetaeva RK, Aksenov SM, Chukanov NV (2011) Crystal structure of schüllerite, a new mineral of the heterophyllosilicate family. Dokl Chem 437:90–94

Rastsvetaeva RK, Aksenov SM, Chukanov NV, Lykova IS, Verin IA (2014) Iron-rich schullerite from Kahlenberg (Eifel, Germany): crystal structure and relation to lamprophyllite group minerals. Crystallography Reports 59(6):867–873

Rastsvetaeva RK, Chukanov NV, Aksenov SM (2016) The crystal chemistry of lamprophyllite related minerals. Eur J Mineral 28:915–930

Rastsvetaeva RK, Dorfman MD (1995) Crystal structure of Ba-lamprophyllite in the isomorphous lamprophyllite-barytolamprophyllite series. Crystallogr Rep 40:951–954

Rastsvetaeva RK, Evsyunin VG, Konev AA (1995) Crystal structure of K-barytolamprophyllite. Crystallography Reports 40:472–474

Rastsvetaeva RK, Sokolova MN, Gusev AI (1990) Refined crystal structure of lamprophyllite. Mineral J 5:25–28 (in Russian)

Saf'yanov YN, Vasil'eva NO, Golovachev VP, Kuz'min EA, Belov NV (1983) Crystal structure of lamprophyllite. Dokl Akad Nauk SSSR 269:117–120 (in Russian)

Sokolova E (2006) From structure topology to chemical composition. I. Structural hierarchy and stereochemistry in titanium disilicate minerals. Can Mineral 44:1273–1333

Sokolova E, Cámara F (2008) From structure topology to chemical composition. III. Titanium silicates: The crystal chemistry of barytolamprophyllite. Can Mineral 46:403–412

Sokolova E, Cámara F (2016) From structure topology to chemical composition. XXI. Understanding the crystal chemistry of barium in TS-block minerals. Can Mineral 54:79–95

Sokolova E, Cámara F (2017) The seidozerite supergroup of TS-block minerals: nomenclature and classification, with change of the following names: rinkite to rinkite-(Ce), mosandrite to mosandrite-(Ce), hainite to hainite-(Y) and innelite-1*T* to innelite-1*A*. Mineral Mag. https://doi.org/10.1180/minmag.2017.081.010

Ulbrich MNC (1993) Mineralogy of nepheline syenites from the Pocos de Caldas alkaline massif, SE Brazil: chemistry, X-ray data and microtextures of feldspars. Rev Bras Geosci 23(4):388–399

Vlasov KA, Kuzmenko MV, Eskova EM (1966) The Lovozero Alkali Massif. Editorial Board of the Academy of Sciences of the USSR Moscow 618 (in Russian)

Wight Q, Chao G (1995) Mont Saint-Hiliare revisited. Rocks and Minerals 70 (pg. 90–103):131–138

Zaitsev VA (2005) Numerical dependence of the unit-cell parameters of minerals of the lamprophyllite group on the cationic composition in the interlayer position. Crystallography Reports 50(3):379–381

Zaitsev VA, Kogarko LN (2002) The compositions of minerals of the lamprophyllite group from alkaline massifs worldwide. Geochem Int 40(4):313–322

Zhirov DV (2015) Geodynamic Reconstruction of the Palaeozoic Kola Alkaline Large Igneous Province. Book of XXXII International Conference: Alkaline Alkaline Magmatism of the Earth Magmatism of the Earth and related strategic metal deposits 148